

Molecular mechanisms of gas surface interactions in hypersonic flow

Ioana Cozmuta¹²

ELORET Corporation³, NASA Ames Research Center, Moffett Field, CA 94086

The present paper addresses the problem of modeling catalytic recombination by calculating surface coverage and recombination coefficients of oxygen and nitrogen on silicon dioxide surfaces from atomistic simulations, using Grand Canonical Monte Carlo (GCMC) and Reactive Force Field Molecular Dynamics (ReaxFF MD). The temperature dependence of these parameters and their sensitivity to the characteristics of the atomistic SiO₂ surface are discussed. Adsorption isotherms are determined for pure oxygen, pure nitrogen, and a mix of oxygen and nitrogen interacting with – (a) crystalline, (b) amorphous, (c) hydrogen-terminated, and (d) oxygen-terminated SiO₂ surface. The energetics and equilibrium constants of adsorption processes are determined. A novel methodology to determine recombination coefficients from ReaxFF MD simulations by calculating surface-mediated recombination events, and characterization of collisions with the solid surface, is proposed and tested. A brief discussion is provided on possible ways to integrate results from atomistic scale simulations within a mesoscale gas-surface interaction (GSI) model presently under development. The GSI model builds upon the classical chemical kinetic theory to provide updated net fluxes for the chemical species interacting with the surface and represents a boundary condition for the mass species conservation for continuum level computational fluid dynamics (CFD) simulations.

I. Introduction

Space vehicles, such as Apollo and Orion, entering Earth's atmosphere at hypersonic velocities are characterized by large free-stream Mach numbers ($M \approx 25$ for return from low Earth Orbit, $M \approx 38$ for lunar return, $M \approx 50$ for direct Mars return), and consequently, by high temperatures (several thousand degrees) in the layer behind the bow shock and at the surface. The high kinetic energy levels, characteristic of atmospheric entry, are dissipated by atmospheric drag, leading to aerothermodynamic heating of the vehicle surface. To reliably size thermal protection systems (TPS), it is critical to understand and quantify the levels of aerothermal heating (due to various thermophysical processes) that the vehicles need to withstand. Physical models employed in current computational fluid dynamics (CFD) codes, such as *DPLR*¹, *LAURA*², etc, account for a number of complex physico-chemical and thermo-chemical non-equilibrium processes such as chemical reactions, energy excitation of vibrational degrees of freedom, heat conduction, radiative heating, surface catalytic properties, etc. in the shock layer. The models employed have parametric uncertainties in reaction rates, thermal relaxation times, transport coefficients, and surface material catalytic efficiencies, etc. These uncertainties translate into uncertainties in predicted levels of aerothermal heating, and consequently, the choice and size of the TPS material(s). Reduction of uncertainties calls for basic research in the physico-chemical foundations of such models, as well as on precise determination of model parameters. Of particular interest, which is addressed in the topic of the present work, is accurate knowledge of the interaction between the TPS surface and the shock-heated, dissociated gas (O- and N-atom, NO recombination for the case of Earth entry).

Atomic species are formed by air dissociating inside the shock and diffuse towards the surface where, due to reduced activation energies, they can recombine, leading to an additional heat flux impinging on the vehicle. If

¹ Senior Research Scientist, ELORET Corporation, icozmuta@mail.arc.nasa.gov. Member AIAA.

² Contact address: Mail Stop 230-3, NASA Ames Research Center, Moffett Field, CA, 94035, 650-604-0993

³ 465 S. Mathilda Avenue, Sunnyvale, CA 94086, 408-732-3028

surface recombination of atomic species occurs, the surface is said to be catalytic. Recombination can be *homogeneous* in which two like atoms recombine into the corresponding molecule, or *heterogeneous* in which two different atoms recombine into a molecule. Depending on the recombination rate and the gas/surface coupling, at least part of the energy of gas dissociation in the shock is deposited on the wall, and can be a significant portion of the total heat load. For example, taking gas phase reactions as reference, 493.58 kJ/mol respectively 941.64 kJ/mol of will be deposited directly onto the surface via homogeneous recombination ($O+O \rightarrow O_2$; $N+N \rightarrow N_2$) and 626.84 kJ/mol via heterogeneous recombination ($N+O \rightarrow NO$). Both recombination rates and surface catalytic reaction models depend strongly on surface characteristics, temperature, and pressure. For hypersonic reentry, typical temperature and pressure at the vehicle surface, range between [300K -2000K] and [0.01 atm – 1atm]. A conservative assumption during the early design phase of a typical atmospheric entry vehicle is that the surface is fully catalytic to atom recombination (and maximum heat flux) – an assumption that can be relaxed later in the design phase.

Amorphous silica (SiO_2) is one of the main ingredients in several reusable (LI900, LI2200, FRSI) and ablative (SLA) thermal protection systems. Silica based tiles are the primary insulation system for the shuttle and their use is intended also for future vehicles³, for example, for the central and forward side of the CEV capsule. Shuttle tiles are made of a rigidized, very-high purity amorphous silica fiber 1.2-4 μm in diameter and up to 1/8 inch long. (Fig. 1). To seal tiles from moisture, the surface is coated with a borosilicate reaction-cured glass (RCG) coating. RCG contains 3-7% boron-oxide (B_2O_3), however, from the point of view of surface catalysis it has been shown to act similarly to pure silicon dioxide.⁴

There are a multitude of studies, using a variety of experimental techniques, investigating surface catalytic properties with respect to oxygen and nitrogen.⁵⁻¹⁹ Experimental determination of oxygen and nitrogen recombination coefficients on fused quartz place their typical values at room temperature around 2.5×10^{-4} for oxygen and 1×10^{-4} for nitrogen.¹² However, the range of reported values in the literature is large, spanning 2 orders of magnitude for both oxygen (4×10^{-6} and 1×10^{-4}) and nitrogen (2×10^{-6} to 2×10^{-4}). Experiments on the space shuttle indicate that reaction rate constants for several materials vary appreciably with increased surface temperature;¹⁴ however, the precise temperature dependence of O and N recombination coefficients is still uncertain. A trend of rising recombination coefficients with increasing temperature seems to exist. Scott¹⁶ concludes that the temperature dependence of the recombination coefficients for oxygen and nitrogen obeys an Arrhenius law, but more accuracy is needed in determining such dependencies, perhaps through the use of well-characterized metals as reference materials. Copeland¹⁹ shows, using a diffusion reactor, that NO formation is important in catalysis on quartz surfaces and that N- and O- atom recombination on surfaces cannot be treated independently. Usually O atoms²⁰ adsorb on the surface and block N-atom active sites, which might act as a mechanism of reducing the number of N_2 molecules being formed by homogeneous catalysis surface reactions. Using a similar diffusion tube technique, Kim and Boudart¹⁸ measured apparent recombination probabilities (which account for a surface roughness factor) for oxygen, nitrogen and hydrogen on silica and suggested that in the low temperature regime (194K to 500K) the loss probability for nitrogen and oxygen did not obey the Arrhenius law but had a more complex behavior.

From the modeling perspective, current computational fluid dynamics (CFD) models are largely based on empiricism, and are quite often specialized to specific gas mixtures. A general model of gas-surface interactions is therefore much needed. Such a model could be incorporated into CFD as part of the surface boundary condition for the mass species conservation equations^{20,21}.

Consider the model depicted schematically in Fig. 2 with S surface sites and atomic species in gas phase denoted by A_i and A_j and molecular species by $A_i A_j$, the following surface processes are relevant to describe catalysis:

1. Atomic adsorption: $A_i + S \rightarrow A_i S$ with rate constant k_{aa} ;
2. Molecular adsorption: $A_i A_j + 2S \rightarrow A_i A_j S_2$ with rate constant k_{am} ;
3. Molecular dissociation and adsorption, with one atom returning into gas phase: $A_i A_j + S \rightarrow A_i + A_j S$ with rate constant k_{acd} ;
4. Molecular dissociation and adsorption, both atoms becoming adsorbed: $A_i A_j + 2S \rightarrow A_i S + A_j S$ with rate constant k_{aad} ;
5. Atomic desorption: $A_i S \rightarrow A_i + S$ with rate constant k_{da} ;

6. Molecular desorption: $A_i A_j S_2 \rightarrow A_i A_j + 2S$ with rate constant k_{dm} ;
7. One adsorbed atom and one atom from gas phase recombine as a molecule which leaves the surface (Ely Rideal mechanism): $A_i + A_j S \rightarrow A_i A_j + S$ with rate constant k_{DER} ;
8. Two adsorbed atoms recombine at the surface and the molecule leaves the surface (Langmuir Hinshelwood mechanism): $A_i S + A_j S \rightarrow A_i A_j + 2S$ with rate constant k_{dLH} ;

Using the classical chemical kinetic theory one can write the net flux mediated by the surface for each of the involved chemical species which, in turn, depends on the dynamics of the species on the active surface sites according to processes 1-8 described above, and on the rate constants associated with each of these processes. By definition, the surface coverage, θ , is the fraction of occupied surface sites which is a temperature and pressure dependent dynamical property of the surface. Similarly, the recombination coefficient, γ , is the ratio of the number of atoms of recombined species due to surface mediated processes to the total number of gas atoms colliding with the surface which also depends on pressure, temperature and surface properties.

From the briefly sketched model above, two strongly coupled global parameters that characterize the elementary processes defining surface mediated recombinations emerge: the surface coverage, θ and the recombination coefficient, γ . Both parameters are strongly influenced by the microscopic (atomic scale) properties of the surface and therefore their molecular based mechanisms need to be addressed.

The present work focuses on investigating surface coverage and recombination coefficients from an atomistic perspective using Grand Canonical Monte Carlo (GCMC) and Reactive Force Field (ReaxFF) Molecular Dynamics simulations. Of particular interest for this study is the adsorption and recombination mechanism of atomic oxygen and nitrogen on silica (SiO_2) surfaces as a function of temperature, pressure and material structural properties. Such simulations have the advantage of considering realistic characteristics of the atomic SiO_2 surface as well as allowing the system to evolve naturally, providing an accurate description of occurring chemical reactions. Adsorption, surface diffusion and catalytic recombination processes are intrinsically coupled. The future integration of molecular based mechanisms with continuum level computational fluid dynamics calculations is also briefly addressed.

II. Theoretical background

The first step of a surface-catalyzed (homogeneous or heterogeneous) reaction is the sticking/adsorption of the reactant molecule to the solid surface, process in which a molecule originating from the gas phase above the surface will experience an attractive potential and, after diffusing towards the surface, will be trapped on it (Figure 2). The adsorbed particle is then called “adsorbate” or “adatom” while the solid surface is called “substrate”. Thus, the competition for adsorption sites on a surface is very important in defining the kinetics of any catalytic reaction. Adsorption is always an exothermic process and as such the enthalpy variation associated with it is negative, $\Delta_{ads}H < 0$. Typical interaction energies between the substrate and the adsorbate are 20 kJ/mol for physisorption and 250-500 kJ/mol for chemisorption. The latter also involves chemical bond formation and it is necessary for homogeneous or heterogeneous recombination to take place. Van der Waals interactions are responsible for the interaction between the incident particle and the substrate. In general this potential assumes that all the adsorption sites on the substrate are identical and that there is a dependence only on the distance and not on the approach angle or the orientation of the incident particle with respect to the surface. The most frequently employed functional forms of the van der Waals interaction are the Lennard-Jones (also called the 6-12 potential) or Morse potentials.

In the following sections Grand Canonical Monte Carlo (GCMC) simulations are employed to characterize adsorption/desorption properties of SiO_2 surfaces with respect to atomic oxygen and nitrogen. Due to the fact that GCMC simulations lack an associated timescale, Reactive Force Field Molecular Dynamics simulations are further employed to identify and describe surface mediated chemical reactions and reaction rates. In general it is assumed that at the edge of the boundary layer, thermal and chemical equilibrium exists²¹. Given that the size of the systems employed in the present simulations is in the order of a few hundred angstroms ($1 \text{ \AA} = 10^{-10} \text{ m}$), it is a reasonable assumption to consider that such equilibrium exists in the vicinity of the surface. This assumption ensures that the requirement of constant chemical potential, μ , under which GCMC simulations are valid, is met and also allows the use of a single system temperature, for both the gas and the surface.

A. Grand Canonical Monte Carlo simulations

The methodology employed in the present study to characterize the adsorption process of oxygen and nitrogen on SiO₂ surfaces is based on the mechanism of chemisorption proposed by Irvine Langmuir in 1916^{22,22} to calculate *adsorption isotherms*. The concept of *adsorption isotherms*, $\theta(p)$, is used to describe the dependence of the surface coverage, θ , of an adsorbed gas on the pressure, p , of the gas above the surface at a fixed temperature, T .

The following assumptions are used in the Langmuir model:

1. all adsorption sites are assumed to be equally “active”;
2. the influence of already adsorbed molecules on lattice sites in the neighborhood is neglected;
3. large molecules are not considered to adsorb on more than one site;
4. an adsorbed molecule is considered the same as a molecule in the gas phase and
5. the adsorbed layer is at most monomolecular (monolayer adsorption).

Given that a dynamical equilibrium exists between the gas molecules and the adsorbed species bound to the surface of the solid, the adsorption process is generally described by the following equation:



where $[A]$ is the concentration of gas phase particle A , $[S]$ is the concentration of vacant adsorption sites on the substrate and $[AS]$ is the concentration of adsorbed species. k_a and k_d are the rate coefficients for adsorption and desorption, respectively. For a situation of dynamic equilibrium, the surface coverage, θ , is time independent, meaning that the rates of adsorption and desorption should be equal. This can be written in terms of pressure using the ideal gas law and surface coverage:

$$k_a[A][S] = k_d[AS] \Leftrightarrow k_a p(1 - \theta) = k_d \theta \quad \text{Eq (2)}$$

From this equation one obtains the following expression for the surface coverage, θ :

$$\theta = \frac{k_a p}{k_a p + k_d} = \frac{bp}{1 + bp} \Leftrightarrow \frac{1}{\theta} = 1 + \frac{1}{bp} \text{ with } b = \frac{K}{k_B T}; \quad \text{Eq (3)}$$

where k_B is the Boltzmann constant ($1.38 \cdot 10^{-23}$ J/K). Eq. 3 provides the relationship between the fractional surface concentration, θ , the equilibrium constant, K and the pressure, p underlying Langmuir’s model of adsorption and establishes that at low pressures the limit for θ is bp while at high pressures θ tends to 1, meaning that all surface sites will be occupied.

Adsorption isotherms can be used to determine not only the concentration of surface sites available for adsorption but also the equilibrium constant, K , for the adsorption-desorption reactions, the enthalpy of adsorption, and, when combined with the rate of gas-surface collisions, the average residence time of a molecule on the surface.

The enthalpy of the adsorption process is equal to the binding energy of the adsorbate-substrate bond. As in most cases the process of surface adsorption is spontaneous, the energy of adsorption, E_a^{ads} is negligible compared to the desorption energy, E_a^{des} (Figure 3). Consequently, the dominant contribution to the enthalpy of adsorption originates from the desorption energy:

$$-\Delta H_{ads} = E_a^{des} - E_a^{ads} \sim E_a^{des} \quad \text{Eq (4)}$$

The relationship between rate and activation enthalpy is provided by the van’t Hoff equation:

$$\left(\frac{\partial \ln K}{\partial T} \right) = \frac{\Delta H_{ads}}{RT^2} \quad \text{Eq (5)}$$

Experimentally the rate constant of desorption from the substrate obeys an Arrhenius like expression:

$$k_d = \tau_0^{-1} e^{-E_{ads}/RT} \quad \text{Eq (6)}$$

indicating that the reciprocal of k_d has units of time and it is actually the average residence time of the adsorbed species on the substrate:

$$\tau = \tau_0 \exp\left(\frac{-\Delta H_{ads}}{RT}\right) \quad \text{Eq (7)}$$

τ_0 represents the collision time between gas particles and the substrate and a typical value is $\tau_0 \approx 10^{-12} \text{ s} = 1 \text{ ps}^{23}$.

While for low pressures (characteristic to hypersonic reentry) the assumption of having monolayer adsorption is most probably valid and the molecules in the shock layer are not large, all the other assumptions made by the model and listed above are difficult to circumvent. However, the Langmuir model of adsorption may be used together with ab-initio based force fields in which case the interactions between the gas species and the surface can be calculated with increased accuracy while at the same time introducing atomic specificity (adsorption sites have distinctive chemistry, gas and adsorbed atoms are characterized by different interaction potentials).

Grand Canonical Monte Carlo (GCMC) simulations represent a computational method customarily employed to determine adsorption isotherms using an atomistic representation of the system. The conserved properties within the GCMC ensemble are the chemical potential, μ , the total system volume, V , and the system temperature, T but not the total number of particles, N . This statistical ensemble, (μ, V, T) , also provides the means to convert the microscopic information to macroscopic observables (pressure, energy, etc). The practical utility of the GCMC ensemble lies in the facts that it closely represents the conditions under which experiments are often performed and that it gives direct access to the equation of state.

During a GCMC simulation, the system is connected to an infinite fictitious reservoir of particles which allows the number of particles, N , to vary occasionally by:

1. particle displacement via translation or rotation;
2. particle destruction;
3. particle creation (random positions);

according to the following probabilities:

$$P_{creation} = \min\left[1, \exp\left(-\frac{\Delta E}{k_B T}\right) - \ln\left(\frac{N_i k_B T}{f_i V}\right)\right] \quad \text{Eq (8)}$$

$$P_{destruction} = \min\left[1, \exp\left(-\frac{\Delta E}{k_B T}\right) - \ln\left(\frac{N k_B T}{f_i V}\right)\right]$$

where ΔE is the energy change between the new and previous configuration, N_i is the current number of molecules of component i in the framework, f_i is the fugacity of component i in the gas phase and V the total cell volume. The stochastic rule for these insertions and removals is such that each one agrees with the thermodynamic probability for that process. Convergence is achieved most rapidly if mechanisms 1-3 listed above occur with approximately equal frequency. Just as in the Canonical Monte Carlo²⁴ procedure, the states within GCMC are sampled in a random manner and a sequence of microstates with the appropriate relative frequencies is produced. The result of the simulation is a set of particle configurations that converge towards the specified pressure/fugacity and temperature. From a set of GCMC simulations the load, L (number of particles/unit cell volume) as function of pressure is determined for various temperatures. The load can easily be expressed in terms of gas volume, V_g that will adsorb onto the surface. If V_m is the volume of gas that corresponds to a monolayer coverage, the surface coverage is

defined by: $\theta = \frac{V_g}{V_m}$. Thus, Eq. 3 may be rewritten in terms of adsorbed gas volume as:

$$\frac{1}{V_g} = \frac{1}{bpV_m} + \frac{1}{V_m}; \quad \text{Eq (9)}$$

From the intercept respectively the slope of a linear fit through $(1/V_g, 1/p)$, the monolayer volume, V_m , and the equilibrium constant, K , (via Eq. 1 and $b = K/k_B T$) are determined. Once the monolayer volume corresponding to

each temperature, T , is calculated, the surface coverage can also be determined. Adsorption isotherms are then defined by plotting the inverse of the surface coverage, θ , as a function of the inverse of the pressure, p . Using the van't Hoff equation (Eq. 5), the enthalpy of adsorption can also be determined.

B. Reactive Force Field Molecular Dynamics

The Molecular Dynamics (MD) method owes its beginning in theoretical physics but gained popularity in material science and, since the 1970s, also in biochemistry and biophysics. Mathematical equations are applied to describe the relationship of chemical structure to energy. In principle, all the properties of a system can then be calculated by combining this information with statistical mechanics. All of the information needed to calculate the dynamics of an isolated system can be determined from the potential energy function $U(\mathbf{r})$ of the system. From Newton's laws, the (conservative) force on atom i in the system can be determined as:

$$F_i = -\nabla_i U(\vec{r}) \quad \text{Eq (10)}$$

The forces are used either to determine the optimum geometry or the dynamics of motion. For the latter scheme, an integrator is then used to calculate the trajectories of the atoms. An exact description, from first principles, would involve solving Schrödinger's equation, for every geometry. However, this is not practical for large systems (more than 1000 atoms), even with the most powerful supercomputer existing today. The overall description of the potential energy and interatomic forces of an N-body system in terms of superposition of simpler terms is provided by a *Force Field*. A force field can be empirical, derived from higher-level modeling (e.g. quantum chemical studies), or even heuristic, and it is independent of the system's electronic configuration. Parameters in the potential may also include a fit against known physical properties of the system being simulated, such as elastic constants and lattice parameters. Actually, early generations of valence force fields were based entirely on experimental data, gas phase structures, and vibrational frequencies. Such empirical parameters cover however only a limited number of functional groups. The recent generation of force fields relies heavily on quantum mechanical calculations to derive the empirical parameters for any type of molecular species. Where highly accurate experimental data are available, the quantum calculations may include corrections from these data.

The basic building blocks of a force field are the expressions of the potential energy function corresponding to the various included interactions as well as the empirical parameters that enter these functionals. Conventional empirical force fields used by standard molecular dynamics programs are considered to be nonreactive, because they employ rigid interatomic connectivity and cannot describe chemical reactions mediated by the surface. The force field employed in the present study (ReaxFF), to examine the gas recombination due to surface catalysis, is of a reactive nature and provides an accurate description of dissociation and reaction curves^{25,26}. The system energy in ReaxFF is divided into partial energy contributions similar to those of empirical nonreactive force fields (bond, angle, torsion, van der Waals, and Coulomb) with the distinction that, in ReaxFF, all these contributions are bond order dependent and the nonbonded interactions (van der Waals and Coulomb) are included for all atom pairs to ensure continuity in the energy description during bond dissociation:

$$E_{system} = E_{val,bond} + E_{val,angle} + E_{val,torsion} + E_{vdWaals} + E_{Coulomb} + E_{lp} + E_{over} + E_{under} + E_{pen} + E_{conj} \quad \text{Eq (11)}$$

The bond order dependence allows a smooth transition from nonbonded to single-, double-, and triple-bonded systems by ensuring that the corresponding energetic contributions disappear upon bond dissociation. To avoid over or undercoordination of the atoms, energy penalties (E_{over} and E_{under}) are imposed on the system. There is a special term, E_{lp} , treating lone-pair electrons on O and N. Other energetic penalties (E_{pen}) may be included to ensure stability of the system. ReaxFF uses a geometry-dependent polarizable charge distribution scheme. The non-bonded interactions (van der Waals and Coulomb) are calculated between all atom pairs, irrespective of connectivity. The van der Waals interactions are described by a distance-corrected Morse potential which includes corrections to avoid energy discontinuities when charged species move in and out of the non-bonded cutoff radius employed by ReaxFF²⁵. The empirical parameters that enter the energy terms in Eq. 11 above were determined by employing a force field optimization procedure using a successive one-parameter search technique on a training set of structures²⁷. In general ReaxFF reproduces heats of formation to within 4.0 kcal/mol, bond lengths to within 0.01 Å

and bond angles to within 2^0 of their literature values and it was validated by comparing its predictions with an extensive set of experimental data and quantum chemistry (DFT) calculations^{25, 26}.

Design of a MD simulation can often encounter limits of computational power. Simulation size and time duration must be selected so that the calculation can finish within a useful time period. The simulation's time duration depends on the length of each time-step, between which forces are recalculated. The time-step must be chosen small enough to have tolerable discretization errors. At the same time the total number of time-steps, i.e. simulation time, must be chosen large enough to capture the effect being modeled without exceeding feasible resources. The simulation size must be large enough to express the effect without the boundary conditions disrupting the behavior. Boundary constraints are often treated by choosing fixed boundary conditions, or by choosing periodic boundary conditions in which one side of the simulation loops back to the opposite side. The scalability of the simulation with respect to the number of molecules is usually a significant factor in the range of simulation sizes that can be simulated in a reasonable time period. Common MD simulations usually scale as $O(N \log(N))$, or, with good use of neighbor lists, $O(N)$, with N as the number of atoms. Another basic limitation of all MD simulations is sampling. With current state of the art MD simulations, time scales longer than 50 ns are not practical and thus, there is no full sampling of all the thermally accessible configurations of a chemical system. Moreover, within such time scales, MD simulations may get trapped in meta-stable conformational states that may not be representative of reality. It is thus important, to follow the convergence of essential system properties.

ReaxFF MD simulations enable following the time evolution of the system: total and component energies, particle positions and velocities, compound occurrence, nature and frequency of chemical reactions. By exploiting such information for simulations targeting hypersonic conditions, it is possible to construct more realistic models of surface catalysis, identifying critical chemical reactions occurring in the system, determining reaction rates, recombination coefficients and their pressure and temperature dependence, characterize surface adsorption/desorption, diffusion, and oxidation and even investigate microscopic mechanisms underlying ablation.

III. Results and Discussions

A. Preparation of atomistic systems

The GCMC and ReaxFF MD simulations are performed on a unit cell that contains a slab of the SiO_2 surface and the atomic oxygen and nitrogen (gas phase) interacting with it. Information from X-ray diffraction data (symmetry group, unit cell parameters and angles and atomic coordinates of the Si and O elements) is normally used to build the bulk solid. The structure of bulk quartz considered in the present study is taken from the Cerius2 data base²⁸. Bulk silicon dioxide (silica) consists of SiO_4 tetrahedra that are bridged together through the oxygen atoms, meaning that each oxygen in the substructure is shared by two silicon atoms. The tetrahedra link together corner to corner and the different rotation angles determine the different existing forms of crystalline silicon dioxide: quartz, cristoballite, etc (Fig. 4). In the amorphous state (a- SiO_2), these tetrahedra are connected to each other in a disordered fashion, and long-range order characteristic of the crystalline phase is lost (Fig. 5). Both crystalline and amorphous silica surfaces exhibit structural properties different from those of the bulk, and uncoordinated oxygen atoms are commonly present. The crystalline surface of SiO_2 is generated by performing a cut along the (001) crystallographic direction of bulk quartz (Fig. 5) while the amorphous silica surface was taken directly from the Cerius2 data base²⁸.

For both structure, the size of the unit cell parameter normal to the surface was increased to accommodate the gas volume corresponding to a certain pressure. Both sides of the surface are exposed to interact with the gas atoms. The crystalline SiO_2 surface considered in the present simulation has an area of 959.4 \AA^2 and a thickness of 11 \AA . The amorphous SiO_2 surface has an area of 812.8 \AA^2 and a slab thicknesses of 19 \AA ($1 \text{ \AA} = 10^{-10} \text{ m}$).

Besides the uncoordinated quartz and the amorphous SiO_2 surfaces, the hydrogen and oxygen terminated versions of the crystalline surface are also considered. The oxygen monolayer surface is investigated to understand how adsorption properties change beyond monolayer adsorption of oxygen. The hydrogen terminated surface is of interest due to the fact that untreated Space Shuttle tiles are well known²⁹ for their tendency to largely adsorb water due to the hydrophilic character of the exposed surfaces. When exposed to air, the silica surface will most probably end up having all the uncoordinated oxygen atoms on the surface become hydroxy groups. To produce a water-repellant surface it is current practice to attach silane molecules (which contain hydrogen) to the surface. For flight

situations, the protective, organic coating is burned off by the heat that is generated upon reentry and as such a hydrogen terminated surface is unlikely to occur. However, it is still of interest for terrestrial test conditions. In what follows, the following simplified notations are used: *c-SiO₂* for the (001) uncoordinated quartz surface, *a-SiO₂* for the amorphous SiO₂ surface, *h-SiO₂* for the hydrogen terminated (001) quartz surface and *o-SiO₂* for the (001) quartz surface with an oxygen monolayer.

B. Adsorption isotherms

Grand Canonical Monte Carlo (GCMC) simulations were performed for the four structures interacting with pure oxygen, pure nitrogen, or a mix (equal proportions) of oxygen and nitrogen gas corresponding to pressures of 0.02 atm to 1.5 atm⁴ and for temperatures of 300K, 500K, 750K, 1000K, 1250K, 1500K, 1750K, and 1900K. Both the pressure and temperature conditions chosen in the present investigations are characteristic for hypersonic reentry of the Space Shuttle.

Within the GCMC simulations, the interactions between the gas (atomic nitrogen and oxygen) and the substrate atoms are evaluated using the Morse-Stretch Charge-Equilibration (MS-Q) Force Field³⁰. The MS-Q Force Field was developed for bulk oxides SiO₂ and Al₂O₃ to model clay minerals and has been successfully employed to model the absorption of organic compounds in calcite³¹. The mathematical forms of the energy functions, useful in averaging over the electronic degrees of freedom, are depicted in Figure 6. One of the important features of this force field is that the atomic charges are allowed to readjust instantaneously to the atomic configurations. These charges are calculated using the charge equilibration (Qeq) method³². To account for short-range non-electrostatic interactions a two-body Morse stretch potential is included. Table 1 and Table 2 contain the MS-Q FF parameters employed in the current modeling corresponding to the diagonal and off-diagonal van der Waals interactions.

For each temperature and pressure, the corresponding equilibrium load is calculated from the GCMC ensemble after 1,000,000 steps. This value is selected on the basis of providing a reasonable number of configurations (Eq. 9) to achieve solution convergence within a short run time (per data point, approximately an hour on one CPU on an SGI Irix machine). Each value of the load is converted into gas volume using the following formula:

$$V_g(p,T) = \frac{Load(p,T) * V_\mu}{N_A} \quad \text{Eq (12)}$$

with $V_\mu = 2.24 \cdot 10^{-2} \text{ m}^3/\text{mol}$ and $N_A = 6.023 \cdot 10^{23} \text{ molecules/mol}$. Using Eq. 9 to plot $(1/V_g, 1/p)$, the monolayer volume and the equilibrium constants are calculated from the intercept and, respectively, the slope of the linear fit. Figure 7 shows the $(1/V, 1/p)$ log-log plots for the pure gases (oxygen and nitrogen) and Figure 8 the corresponding plots for oxygen and nitrogen in the equal proportion mix. For all the cases, the error bars are within the data points. For some instances of oxygen in the mix, interacting with *h-SiO₂* and *o-SiO₂* and for a combination of small pressures and high temperatures, the number of statistical events generated during the GCMC simulations was very low and led to large fluctuations. The corresponding (V_g, p) plots exhibited a strong deviation from the expected linear behavior and the entire data set was excluded from the analysis. Given such considerations, the rest of the linear fits to the data points were performed with values of R^2 between 0.85 and 0.99. Future investigations will address GCMC simulations for the excluded data sets to better understand the origin of the low statistical events.

Conversely, using Eq. 12 one can determine the number of molecules/atoms corresponding to the monolayer volume. The number of adsorption sites corresponding to the monolayer volume is determined assuming a one to one correspondence between the number of adsorption sites and the number of adsorbed atoms. This value only depends on temperature while the pressure only influences how much of the monolayer volume is occupied, and determines the occupancy, θ . The temperature dependence of the number of sites per SiO₂ area (*c-SiO₂*, *a-SiO₂*, *h-SiO₂*, and *o-SiO₂*) for pure oxygen, pure nitrogen, and equal proportions of oxygen and nitrogen gas in a mix is shown in Figure 9. The monolayer volume is in all cases largest at 300K and decreases with increasing temperature. This behavior is expected given that at higher temperatures the gas atoms have higher velocities and thus will adsorb less. For pure oxygen gas interacting with SiO₂ there is a larger number of adsorption sites on the amorphous than

⁴ For the oxygen-nitrogen gas mix the partial pressures of the gas species are considered.

on the crystalline surface (Fig 9, top-left). A hydrogen or oxygen terminated SiO₂ surface, however, strongly reduces the number of adsorption sites for oxygen, especially at temperatures larger than 500K.

For pure nitrogen gas, the number of adsorption sites at 300K exceeds that of oxygen for a hydrogen terminated surface. The crystalline surface then exhibits a larger number of adsorption sites than the amorphous or oxygen terminated surface. For temperatures above 500K the number of adsorption sites for nitrogen in both pure gas and in a mix with oxygen is strongly decreased. Naturally, in the gas mix, because of the existing competition between oxygen and nitrogen to occupy surface adsorption sites, the number of adsorption sites for each species is smaller than compared to the pure gas. However, the number of adsorption sites available for oxygen, especially between temperatures of 500K to 1250K, dominates over nitrogen.

Once the volume of the monolayer is calculated, from the slope (Eq. 10) one determines the equilibrium constant K. The utility of K is realized by noting that if K is large ($k_a \gg k_d$) then equilibrium lies to the right of Eq. 1 (in the gas phase) while if K is small ($k_a \ll k_d$) then equilibrium lies to the left of Eq. 1 (on the surface). Figure 10 shows the dependence of K for pure oxygen, pure nitrogen, and oxygen and nitrogen in equal proportion on the four SiO₂ surfaces under study. The equilibrium constant for the pure oxygen gas adsorption on a-SiO₂ surface exhibits a sharp increase from 300K to 750K followed by a peak value at ~750K, indicating that for this temperature regime the desorption rate, k_d , is approximately a factor of 10 faster than the adsorption rate, k_a . Oxygen has a similar behavior in the O/N mix with the difference that the peak value of K occurs around ~500K, most probably due to the presence of nitrogen.

Overall, for nitrogen the equilibrium constants, K, are two orders of magnitude smaller. The presence of peaks occurs at higher temperatures (>1000K) for the a-SiO₂ in the pure nitrogen gas and both a-SiO₂ and o-SiO₂ in the O/N mix.

Fig. 11 to Fig. 19 show the binding sites represented as “mass clouds” of points colored by energy for the four surfaces and for pure oxygen and pure nitrogen (Fig. 11 to Fig. 14) as well as for the O/N mix (Fig. 15 to Fig. 18). A top view of the distribution of binding sites corresponding to 300K for 0.01 atm and 1atm for the four surfaces is also given in Fig. 19. The following conclusions are suggested by these images:

- For both oxygen and nitrogen (in pure gas or in the mix) the number of adsorption sites decreases with increasing temperature and decreasing pressure.
- The number of adsorption sites for oxygen is significantly larger than the number of adsorption sites for nitrogen
- The adsorption sites for oxygen are also more energetic than for nitrogen. At 300K and 1atm, typical energies for oxygen for the c-SiO₂ surface are in the range [-16, -10] kcal/mol while the corresponding values for nitrogen range between [-0.6, -0.4] kcal/mol. Binding energies of oxygen on a-SiO₂ are more negative, ranging between [-30, -25] kcal/mol. Both h-SiO₂ and o-SiO₂ are characterized by elevated binding energies, in the order of [-8, -5] kcal/mol. For oxygen, with temperature increase, the binding energies decrease strongly for the crystalline SiO₂ surface, reaching a value of -2.2 kcal/mol at 1900K. For the same pressure, the binding energies for h-SiO₂ at high temperatures are about one order of magnitude smaller than at 300K.
- Due to the fact that a-SiO₂ is more porous than c-SiO₂, adsorption also occurs inside the voids exhibited by the solid structure (Fig. 12, Fig. 16). This is also the reason for more negative binding energies characteristic of oxygen and nitrogen in a-SiO₂ and a reduced variation with increasing temperature of such binding energies.
- Characteristic for oxygen adsorption on SiO₂ is the presence of hot spots on the surface of the material while for nitrogen the distribution of adsorption sites is relatively uniform (Fig. 11-Fig. 14)
- In the O/N mix oxygen adsorption dominates over nitrogen and the presence of oxygen lowers the binding energies for nitrogen as well.
- The top view of the distribution of adsorption sites (Fig. 19) indicates the presence of several adsorption “hot” spots in c-SiO₂ and a-SiO₂ while such adsorption sites are almost absent for the case of h-SiO₂. For o-SiO₂ the number seems comparable with that for c-SiO₂ however with increased (less negative) binding energies.

Finally, adsorption isotherms representing the variation of surface occupancy with temperature (plotted as $1/\theta$ versus $1/p$) are calculated and shown in Fig. 20 for pure oxygen and pure nitrogen and in Fig. 21 for the O/N mix. Close to 300K and for large pressures (1-1.5 atm) the surface occupancy reaches the monolayer volume. For pure oxygen and

nitrogen, the highest occupancy is achieved for the amorphous SiO₂ surface (Fig. 20) while for the oxygen in the O/N mix the highest occupancy is reached for the amorphous as well as for the oxidized o-SiO₂. Nitrogen in the O/N mix is highest for the crystalline and oxidized SiO₂. For pure oxygen the occupancy decreases with temperature such that around 1500K it is the lowest, while the 1900K isotherm indicates a slight increase in occupancy. For pure nitrogen, a similar trend is observed except that for high temperatures the occupancy is comparable to that corresponding to 300K or may even be exceeded (Fig. 20, h-SiO₂ and o-SiO₂). This trend is also seen in the O/N mix where for crystalline SiO₂ the presence of oxygen in the mix (compared to the pure gas) leads to an increased occupancy for nitrogen (Fig. 21, top) and a decreased occupancy for the amorphous phase (Fig. 21, second row). For both hydrogen and oxygen terminated crystalline SiO₂ surfaces, the presence of oxygen in the mix acts like a catalyst for nitrogen adsorption.

In general the GCMC simulations show that the dynamics of adsorption of oxygen and nitrogen atoms in the mix versus pure gases on the SiO₂ surfaces is significantly affected by the combined presence of the two atomic species which agrees with the observations by Copeland¹⁹.

Such adsorption isotherms can be used to build mesoscale gas-surface interaction models as they provide quantitative determinations of occupancy values for a wide pressure-temperature landscape.

C. Heterogeneous recombination

For the MD runs, simulations were performed only for the oxygen-nitrogen gas mix on c-SiO₂ and a-SiO₂ and for the same temperatures as used in the GCMC simulations. To correctly account for the change in gas volume corresponding to various pressure and temperature conditions while preserving the same number of particles (40 oxygen atoms and 40 nitrogen atoms) to provide statistical data, the unit cells were constructed using the volumes predicted by the ideal gas law and considering the thickness of the SiO₂ slab. The employed unit cell volumes and corresponding densities, for pressures of 100 atm and 10 atm, are indicated in Table 3. The areas of the crystalline and amorphous SiO₂ surfaces considered in the MD simulations at 100 atm are 959.4 Å² and 812.8 Å², respectively. At lower pressures (10 atm), to accommodate the same number of molecules while keeping the same size of the SiO₂ surfaces, the height of the gas column on top of the surface would have become disproportionately large than the other two unit cell dimensions. Thus, the SiO₂ surface was increased to 4 times the original size (3837.3 Å² for c-SiO₂ and 3251.3 Å² for a-SiO₂). An integration time step of 0.3 fs was used throughout the ReaxFF MD simulations. Before entering the production phase of the MD simulations, each system was equilibrated via 50 ps of NPT dynamics followed by 50 ps of NVT dynamics. All the production runs were generated using NVT dynamics for 1000000-2000000 steps (equivalent to 300-600ps). The serial version of ReaxFF was used in the present simulations on the Altix2 architecture (Columbia supercomputer) at NASA Ames Research Center. However, a number of 8 CPU's per run was used to provide the necessary memory resources for the simulated systems. To run 1000000 steps of ReaxFF-MD required about one week of computer time (8CPU's).

In the present paper only the high-pressure case (10 atm, 100atm) will be discussed. The purpose of performing the ReaxFF simulations at pressures elevated compared to hypersonic relevant conditions is to ensure the presence of heterogeneous recombination events, especially that of NO and to be able to use such calculations to “calibrate” our analysis.

Fig. 22 captures a snapshot of the ReaxFF dynamics of oxygen and nitrogen on crystalline SiO₂ at 1900 K and 100 atm. There is evidence of stable molecular oxygen and nitrogen formation in the gas phase. NO recombination exists in the gas phase as well as surface mediated, with surface mediated events dominating over gas recombination. Exotic species such as N₂O and NO₂ are also being formed mostly in the vicinity of the solid surface. Some of the surface mediated recombined molecules, before returning to the gas phase, may spend several picoseconds in the neighborhood of the surface in a transitory state between the recombined and the surface adsorbed state. For example, several events have been observed along the ReaxFF MD trajectory in which the oxygen atom, already adsorbed on the surface, goes several times through the same transitory states between forming a bond with a nitrogen atom originating from gas phase and keeping its bond with the surface Si atom until finally, gaining enough energy, it leaves the surface as a recombined NO species.

The compound occurrence during the ReaxFF simulations for the c-SiO₂ as a function of temperature is shown in Fig. 23. Here the dynamics of the gas phase (oxygen, nitrogen, and formation of molecular species such as O₂, N₂)

as well as that of the surface (surface oxygen and nitrogen) is followed. The main trend to be extracted from these simulations is that there is a stronger oxygen adsorption on the surface as compared to nitrogen and a significant amount of molecular nitrogen forming in the gas phase. Even at such elevated pressures the number of ON events is relatively small compared to the overall number of occurring events (adsorption, collision with the surface, etc.). It is noticeable however that there is a wide range of N_xO_y types of compounds that form, such as ON_2 , N_2O , O_2N_4 , O_3N , ON_3 , ON_4 , ON_5 , O_2N_3 , O_3N_2 . Such compounds are short lived and their number is significantly smaller than that of, for example, molecular N_2 formation. A more detailed analysis accounts only for the occurrence of surface-mediated events and is shown in Fig. 24. Again, the dominant events, especially for the 10atm pressure, are nitrogen and oxygen adsorption and desorption which occur in comparable amounts with the adsorption mechanisms slightly dominating.

The recombination coefficient is defined by:

$$\gamma = \frac{\text{flux of atoms recombining at the surface}}{\text{flux of atoms impinging on the surface}} \quad \text{Eq (13)}$$

The number of surface mediated ON events is determined by analyzing the surface dynamics and counting for events in which an adsorbed oxygen and an adsorbed nitrogen leave the surface. This should coincide at the same time with the appearance of an ON molecule into the gas phase.

To count the total number of nitrogen and oxygen collisions with the surface, the following strategy is employed:

- From the MD trajectory, the time evolution of the gas atoms' coordinates is extracted
- Events are identified in which a change in sign of the variation of the position vector occurs. Three time steps are considered: $t-1$, t and $t+1$. The initial change in position vector is calculated as:

$$\Delta r_{old} = r(t) - r(t-1) \quad \text{Eq (14)}$$

This change is then used as reference for the new change in position vector:

$$\Delta r_{new} = r(t+1) - r(t) \quad \text{Eq (15)}$$

If there is a change in sign between Δr_{old} and Δr_{new} , this event is counted as collision. However, to avoid counting collision events occurring in the gas phase, such changes in sign need to happen within a certain distance from the surface.

- Given that the surface is defined by moving atoms, the surface of SiO_2 is defined by determining the maximum and minimum coordinate along the SiO_2 width and subtracting a certain tolerance. In the present paper a value of 1.5\AA was employed for the tolerance used to define the upper and lower limits of the solid surface.
- If the sign change stays within 5\AA of the surface for more than 20 ps, the event is counted as being surface diffusion
- If the sign change occurs within 5\AA of the surface but the atom continues to drift away from the surface, the event is counted as surface collision.

The results of total, nitrogen and oxygen collision counts as functions of temperature is shown in Figure 25 for both 100atm and 10atm pressures. With temperature increase, due to the presence of more energetic particles, the number of collisions with the solid surface is higher, a smaller percentage being readily adsorbed. For the same temperature regime, nitrogen collisions with the surface are also more frequent than those of oxygen. Correlated with the adsorption events in Fig. 24 it is indicative of the oxidation process taking place on the SiO_2 surface. In addition, the number of collisions with the surface is smaller at lower pressure (10 atm).

At pressures of 10 atm and 100atm the formation of N_xO_y compounds is also observed (Fig. 23). As such, using Eq. 13, several recombination coefficients were defined and calculated:

$$\gamma_{NO} = \frac{\text{number of NO recombination events}}{\text{number of N collisions with the surface}} \quad \text{Eq (16)}$$

$$\gamma_{ON} = \frac{\text{number of ON recombination events}}{\text{number of O collisions with the surface}} \quad \text{Eq (17)}$$

$$\gamma_{N_xO_y} = \frac{\text{number of } N_xO_y \text{ recombination events}}{\text{total number of N and O collisions with the surface}} \quad \text{Eq (18)}$$

Preliminary calculations of recombination coefficients for ON and N_xO_y use the information from Fig. 24 and Fig. 25. For NO, the recombination coefficient ranges between $[3 \cdot 10^{-3}; 7 \cdot 10^{-2}]$ at 100 atm and between $[3 \cdot 10^{-3}; 4 \cdot 10^{-2}]$ at

10 atm. The recombination coefficient for N_xO_y is about one order of magnitude larger than that calculated for NO, at both 100 atm [$2 \cdot 10^{-2} : 3 \cdot 10^{-1}$] as well as 10 atm [$3 \cdot 10^{-3} : 6 \cdot 10^{-2}$]. The lower the pressure, the smaller the number of N_xO_y events and thus the smaller the value for $\gamma_{N_xO_y}$ (eventually, the number of surface mediated N_xO_y recombinations will become zero at lower pressures).

ReaxFF simulations at 100atm and over the same temperature range were repeated for the amorphous SiO_2 . Fig. 26 indicates similar chemistry and compound occurrence for amorphous SiO_2 as for crystalline SiO_2 (see Fig. 23). However, the adsorption of both oxygen and nitrogen on amorphous SiO_2 is stronger than for crystalline SiO_2 as also indicated in Fig. 27 and in agreement with the predictions of the GCMC simulations discussed earlier, although at lower pressures.

To perform ReaxFF MD simulations to calculate realistic values of the recombination coefficients is challenging for the following reasons:

1. The size of the simulation cell and the surface of the substrate need to be chosen such that enough statistical collision and recombination events are gathered within reasonable MD time scales;
2. The number of particles in gas phase (oxygen and nitrogen atoms) if too small will lead to particle adsorption on the surface and quick depletion of the gas phase. If on the other hand, new gas particles are artificially added to the gas phase to ensure a constant number of gas atoms, the system pressure is not anymore the same and the overall equilibrium is perturbed.
3. Although the systems are energy equilibrated and have reached constant potential energy, 300-500ps of ReaxFF MD does not seem to provide enough statistics for surface mediated recombinations. Within such time scales a strong correlation seems to exist between the duration of the MD simulations and the calculated values for the recombination coefficients. Study of the influence of the duration of the MD run on such values is presently ongoing.

ReaxFF MD simulations are however useful for the development of gas-surface interaction models by providing the type of chemical reactions that are characteristic to a surface at certain pressure-temperature conditions. Future ReaxFF MD simulations aim to perform a more thorough analysis of the present data, address the lower pressure regime [0.5atm-1atm], characterize surface adsorption sites, their energetics, calculate reaction rates and determine adsorption isotherms for comparison with GCMC generated ones.

D. Concluding Remarks and Future Work

Section IIIB of this paper shows that GCMC simulations represent a fast way of generating adsorption isotherms to provide information related to the temperature, pressure and surface characteristics dependence of surface coverage for pure chemical species or interacting within a gas mixture. This information can be stored in a database to be used in the adequate rate equations for surface species concentrations.

Using the Langmuir isotherm as the underlying description of gas adsorption on a solid surface, a discussion of the reaction/recombination processes (1-8) listed in section 1 would be as follows:

- The Langmuir-Hinshelwood (L-H) mechanisms in which two adatoms located on adjacent surface sites recombine and desorb as a molecule predicts the following dependence of the recombination desorption rate on pressure:

$$Rate = k_c \theta^2 = k_c \frac{b^2 p^2}{1 + 2bp + b^2 p^2} \quad \text{Eq (19)}$$

- At low temperatures the surface is fully covered with adsorbed atoms, $\theta \sim 1$ and $Rate = k_c \theta^2 = k_c$, meaning that the recombination-desorption process is independent of pressure.
- At high temperatures the surface is sparsely covered with adatoms, $\theta \ll 1$, and also $bp \ll 1$ leading to $\theta = bp$ and $Rate = k_c \theta^2 = k_c (bp)^2 = k_c b^2 p^2$ making the recombination-desorption rate second order dependent on gas pressure.
- Adatoms are slowly adsorbed, then migrate rapidly on the surface, and finally recombine with other adatoms, resulting in a molecule which then desorbs. This mechanism is called the Migration Mechanism, and it represents a correction to the L-H mechanism, especially to the kinetics of

adsorption (which is first order dependent on pressure over a wide temperature range). The rate corresponding to this corrected L-H mechanism remains invariant relative to changes in temperature: $Rate = k_c p(1 - \theta)$ or for $\theta \ll 1$, $Rate = k_c p$.

- The Langmuir-Rideal (L-R) or Eley-Rideal mechanism -in which a gas phase atom forms an adatom while another gas phase atom strikes and recombines with the adatom forming a molecule which then desorbs immediately following the recombination and leaving a vacant surface site- predicts the following rate for this process: $Rate = k_c p \theta = k_c p \frac{bp}{1 + bp} = k_c \frac{bp^2}{1 + bp}$. This new expression for the recombination-desorption rate shows a first order dependence on pressure at low temperatures ($Rate = k_c p$) and a second order dependence on pressure for high temperatures ($Rate = k_c bp^2$). However, it does not explain the heterogeneous recombination of atoms on surfaces and does not provide an explanation of the transition of the $Rate$ from first to second order dependence in pressure with temperature increases.

Although from the engineering standpoint, a direct coupling of GCMC and ReaxFF into CFD is, at this time, not a viable solution, the Langmuir model with its statistical GCMC implementation, provides a modality of feeding atomistic determined parameters into mesoscale gas-surface interaction models by empirically fitting such data. The same approach may be used to input rate constants, recombination coefficients and surface occupancy determined from ReaxFF simulations. The advantage of ReaxFF over GCMC simulations consists in the fact that it has a time scale associated to all the incurring processes which however, make such calculations computationally quite expensive. One difficulty, which should be carefully considered, originates from the fact that atomistic simulations usually address surfaces of a few hundred angstroms in size. Such surfaces are representative for the mesoscale length domain (μm) for metals and crystalline matter. For composite or amorphous materials (Fig. 1), microstructural properties such as surface area and porosity play an important role and their values (which could be determined from experimental investigations or digital image analysis) need to be factored in.

Acknowledgments

This work was performed under NASA contract NNA04C25C to ELORET Corporation. The author would like to thank Dr. D. Prabhu, Dr. A. Wray, Dr. R. Jaffe and Dr. D. Bose for valuable insights on the present manuscript. Dr. R. Jaffe has also participated in the earlier stages of this project and his help in generating the crystalline SiO_2 surface is gratefully acknowledged. I would also like to thank Dr. A. C. T. van Duin and Dr. S. Zybin of MSC, Caltech for their continuous support with ReaxFF resources.

Table 1. Diagonal van der Waals parameters from the MS-Q force field. The first column of the table indicates the atom types corresponding to hydrogen (H_C), oxygen in SiO₂ (O_AC), oxygen gas atoms (O_3C), nitrogen gas atoms (N_3) and silicon atoms (Si3C).

Atom	Potential	R ₀	D ₀
H_C	Lennard Jones 6-12	3.195	0.0152
N_3	Lennard Jones 6-12	3.662	0.0774
O_3C	Lennard Jones 6-12	3.4046	0.0957
O_AC	Morse	3.759	0.1772
Si3C	Morse	3.4013	0.2956

Table 2. Off-diagonal van der Waals parameters from the MS-Q force field. Atoms are indicated using the nomenclature for atom types: hydrogen (H_C), oxygen in SiO₂ (O_AC), oxygen atoms (O_3C), nitrogen gas atoms (N_3) and silicon atoms (Si3C). Geometric combination rules are used for interactions where parameters are not specified.

Atom	Atom	Potential	R ₀	D ₀
O_3C	H_C	Morse	1.0770	19.550
O_AC	H_C	Morse	2.1768	0.1753
O_AC	O_3C	Morse	3.7913	0.5563
O_AC	N_3	Morse	3.7261	0.2040
Si3C	O_3C	Morse	1.6248	45.9982
Si3C	O_AC	Morse	1.6248	45.9982
Si3C	N_3	Morse	3.7106	0.1171

Table 3. Scaling of unit cell volumes and densities for crystalline (c-SiO₂) and amorphous (a-SiO₂) SiO₂, corresponding to gas pressures (atomic oxygen and nitrogen) of 100atm and 10atm, respectively and temperatures of 300K to 1900K. The volumes were scaled using the ideal gas law and considering the thickness of the SiO₂ slab.

T (K)	P (atm)	V(Å ³)		ρ (kg/dm ³)		P (atm)	V(Å ³)		ρ (kg/dm ³)	
		c- SiO ₂	a-SiO ₂	c- SiO ₂	a-SiO ₂		c- SiO ₂	a-SiO ₂	c- SiO ₂	a-SiO ₂
300	100	61205	65025	0.42	0.5	10	546434	559220	0.16	0.21
500		94781	98351	0.27	0.33		880281	894102	0.10	0.13
750		136608	140617	0.19	0.23		1302386	1313527	0.07	0.09
1000		178818	182071	0.14	0.18		1720654	1732932	0.05	0.07
1250		220070	224338	0.12	0.15		2138922	2149096	0.04	0.06
1500		262280	265792	0.1	0.12		2557190	2568511	0.04	0.05
1750		304491	308058	0.08	0.11		2994644	2987926	0.03	0.04
1900		329433	333256	0.08	0.1		3228721	3241526	0.03	0.04

References

1. Wright, M. J. C., G. V.; and Bose, D., Data Parallel Line Relaxation Method for the Navier Stokes Equations. *AIAA Journal*, **1998**, 36(9), 1603-1609.
2. Cheatwood, F. M. and Gnoffo, P. A., User's Manual for the Langley Aerothermodynamic Upwind Algorithm (LAURA). *NASA TM-4674*, **1996**.
3. Sietzen, F. Jr., Cooling off Orion's fiery return. *Aerospace America*, **2007**, 28-32.
4. Jumper, E. J. and Seward, W. A., Model for Oxygen Recombination on Reaction Cured Glass. *Journal of Thermophysics and Heat Transfer*, **1994**, 8(3), 460-465.
5. Greaves, J. C. and Linnett, J. W., The Recombination of Oxygen Atoms at Surfaces. *Transaction of the Faraday Society*, **1958**, 54, 1323-1330.
6. Greaves, J. C. and Linnett, J. W., The Recombination of Oxygen Atoms at Surfaces. *Transaction of the Faraday Society*, **1958**, 54, 1323-1330.
7. Greaves, J. C. and Linnett, J. W., Recombination of atoms at surfaces. *Transactions of the Faraday Society*, **1959**, 55.
8. Halpern, B. and Rosner, E. E., Chemical Energy Accommodation at Catalyst Surfaces. *Chemical Society, Faraday Transactions*, **1978**, 74, 1833-1912.
9. Kaufman, F., *J. Chem. Phys*, **1958**, 28, 352-.
10. Stewart, D. A., Chen, Y. K. and Henline, W. D., Effect of Non-Equilibrium Flow Chemistry and Surface Catalysis on Surface Heating to AFE. *AIAA 26th Thermophysics Conference, Honolulu, Hawaii* **1991**.
11. Kolodziej, P. and Stewart, D. A., Nitrogen Recombination on High-Temperature Reusable Surface Insulation and the Analysis of its Effect on Surface Catalysis. *AIAA 22nd Thermophysics Conference, Honolulu, Hawaii* **1987**.
12. Marschall, J., Experimental Determination of Oxygen and Nitrogen Recombination Coefficients at Elevated Temperature Using Laser-Induced Fluorescence. *1997 National Heat Transfer Conference, Baltimore, MD* **1997**.
13. Scott, C. D. and Derry, S. M., Catalytic Recombination and the Space Shuttle Heating. *AIAA/ASME 3rd Joint Thermophysics, Fluids, Plasma and Heat Transfer Conference, St. Louis, Missouri*, **1982**.
14. Stewart, D. A., Rakich, J. V. and Lanfranco, M. J., Catalytic Surface Effects Experiment on Space Shuttle. *AIAA 16th Thermophysics Conference*, **1981**.
15. Cook, S. R., Cross, J. B. and Hoffbauer, M., Hypersonic Gas-Surface Energy Accommodation Test Facility. *18th AIAA Aerospace Ground Testing Conference* **1994**.
16. Scott, C. D., Catalytic Recombination of Nitrogen and Oxygen on High-Temperature Reusable Surface Insulation. *AIAA 15th Thermophysics Conference* **1980**.
17. Sepka, S., Copeland, R., Marschall, J. and Chen, Y. K., Experimental Investigation of Surface Reactions in Carbon Monoxide and Oxygen Mixtures. *AIAA 33rd Thermophysics Conference* **1999**.
18. Kim, Y. C. and Boudart, M., Recombination of O, N, and H Atoms on Silica: Kinetics and Mechanism. *Langmuir*, **1991**, 7, 2999-3005.

19. Copeland, R. A., Pallix, J. B. and Stewart, D. A., Surface-Catalyzed Production of NO from Recombination of N and O Atoms. *Journal of Thermophysics and Heat Transfer* **1998**, 12(4), 496-499.
20. Reggiani, S., Barbato, M., Bruno, C. and Muylaert, J., Model for Heterogeneous Catalysis on Metal Surfaces with Applications to Hypersonic Flows. *Journal of thermophysics and heat transfer*, **1996**, 14(3), 412-420.
21. Armenise, I., Barbato, M., Capitelli, M. and Kustova, E., State-to-State Catalytic Models, Kinetics and Transport in Hypersonic Boundary Layers. *Journal of Thermophysics and Heat Transfer* **2006**, 20(3), 465-476.
22. Langmuir, I., Surface chemistry. *Nobel lecture* **1932**.
23. McQuarrie, D. A. and Simon, J. D., Physical Chemistry -a molecular approach. *University Science Books, Sausalito, CA* **1997**.
24. Allen, M. P. and Tildesley, D. J., Computer Simulation of Liquids. *Oxford Science Publications* **1997**.
25. van Duin, A. C. T., Dasgupta, S., Lorant, F. and Goddard, W. A. III, ReaxFF: A Reactive Force Field for Hydrocarbons. *J. Phys. Chem. A* **2001**, 105, 9396-9409.
26. van Duin, A. C. T., Strachan, A., Stewman, S., Zhang, Q., Xu, X. and Goddard, W. A. III, ReaxFF SiO reactive force field for silicon and silicon oxide systems. *J. Phys. Chem. A* **2003**, 107, 3803-3811.
27. van Duin, A. C. T., Baas, J. M. A. and van der Graaf, B., Delft Molecular Mechanics: A New Approach to Hydrocarbon Force Fields. *J. Chem. Soc. Faraday Trans.* **1994**, 90, (19), 2881-2895.
28. Accelrys Inc., Cerius2 MSI Manual. *San Diego, CA* **1997**.
29. Fisher, R. M. and Dalton, P., Hygroscopic Characteristics of Space Shuttle Tiles. *NASA Contractor Report 177475* **1987**.
30. Demiralp, E., Cagin, T. and Goddard, W. A. III, The MS-Q force field for ceramics: application to the quartz-stishovite phase transition and to silica glass. *Physical Review Letters* **1999**, 82, (8), 1708-1711.
31. Hwang, S., Blanco, M., Demiralp, E., Cagin, T. and Goddard, W. A. , The MS-Q Force Field for Clay Minerals: Application to Oil Production. *J. Phys. Chem. B* **2001**, 105, (19), 4122-4127.
32. Rappe, A. K. and Goddard, W. A. III, Charge equilibration for molecular dynamics simulations. *Journal of Physical Chemistry* **1991**, 95, 3358-3363.

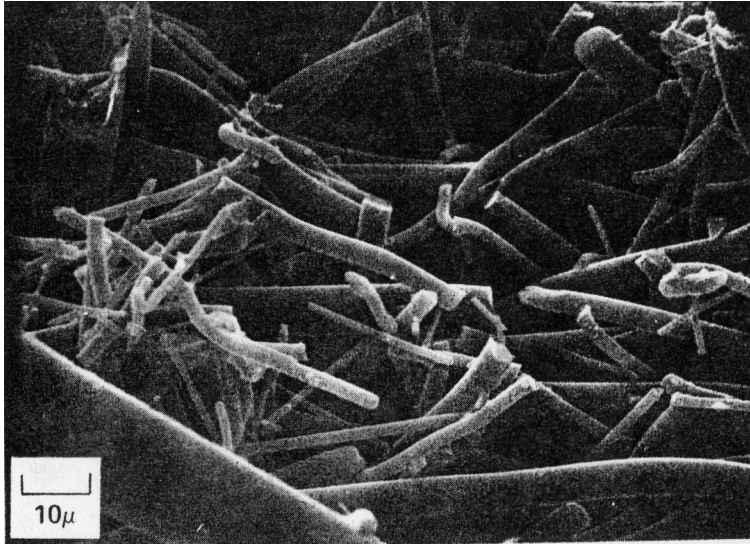


Figure 1. Microstructure of silica LI2200.

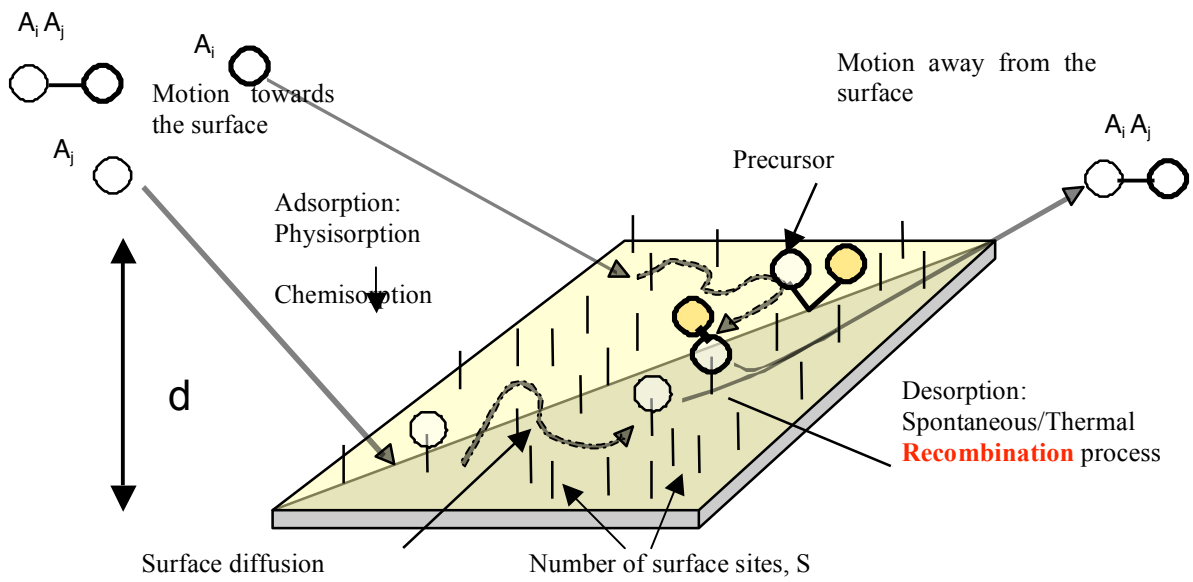


Figure 2. Schematic representation of several gas-surface interactions mechanisms.

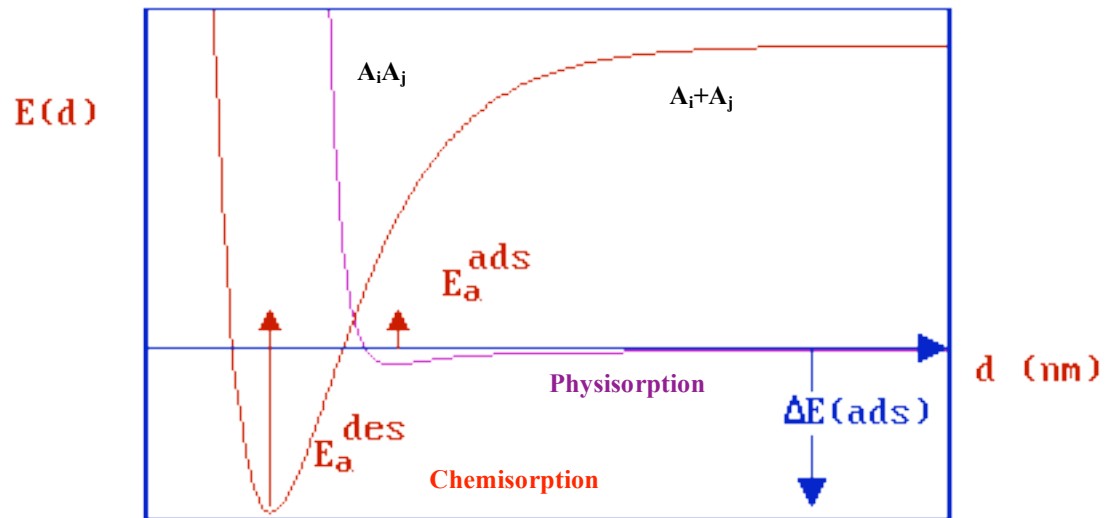


Figure 3. Energetic barriers for physisorption and chemisorption.

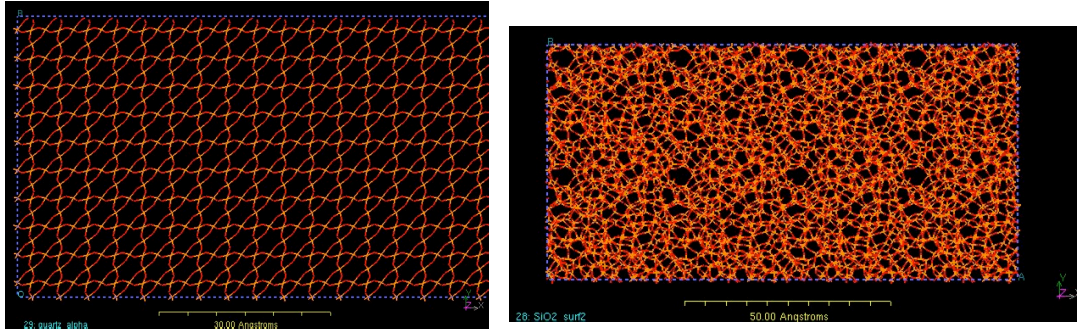


Figure 4. Atomistic structure of bulk crystalline quartz (left) and amorphous (right) SiO_2 .

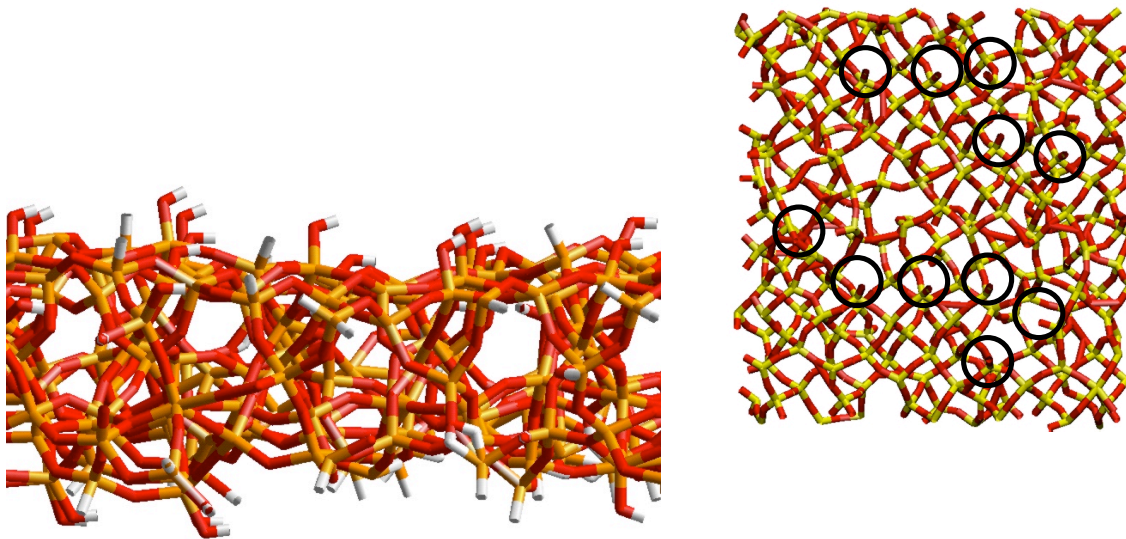
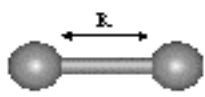
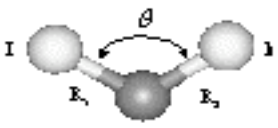
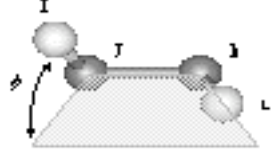
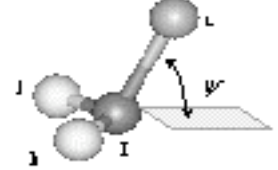


Figure 5. Left: Atomistic model of a 001 quartz (SiO_2) surface with surface oxygen atoms (red) coordinated with hydrogen atoms (white). Silicon atoms are colored in orange. For the oxygen monolayer structure the hydrogen atoms were replaced by oxygen atoms (not shown). Right: Top view of the 001 uncoordinated SiO_2 surface. The location of a few uncoordinated oxygen atoms is indicated with black circles.

Valence Force Field

Description	Illustration	Typical Expressions	
		Potential	Forces
Bond Stretch		$U_s = \frac{1}{2} K_s (R - R_0)^2$	$-\frac{\partial U}{\partial R} = K_s (R - R_0)$
Bond Angle bend		$U_\theta = \frac{1}{2} C (\cos \theta - \cos \theta_0)^2$	$-\frac{\partial U}{\partial \theta} = C (\cos \theta - \cos \theta_0) \sin \theta$
Torsion		$U_\phi = \sum_{k=1}^n \frac{1}{2} K_{\phi,k} [1 - d \cos(k\phi)]$	$-\frac{\partial U}{\partial \phi} = \frac{1}{2} K_s \cdot d \cdot k \cdot \sin(k\phi)$
Inversion		$U_\psi = \frac{1}{2} C (\cos \psi - \cos \psi_0)^2$	$-\frac{\partial U}{\partial \psi} = C (\cos \psi - \cos \psi_0) \sin \psi$

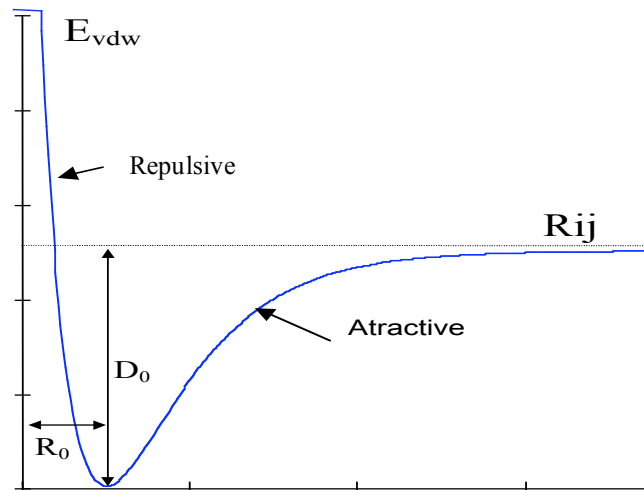


Figure 6. MSQ force field energy expressions.

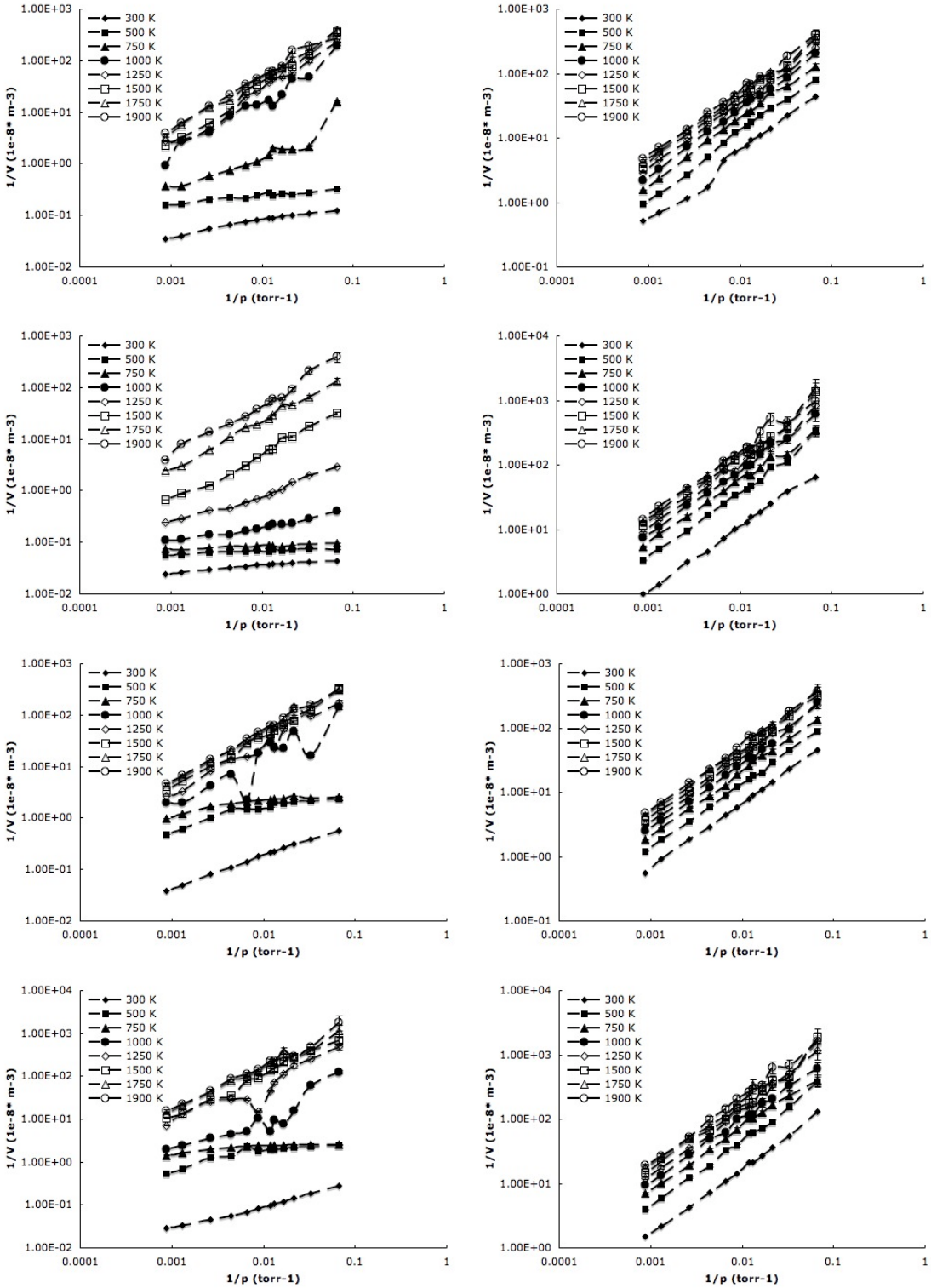


Figure 7. Log-Log plots of $(1/V, 1/p)$ for pure oxygen (left column) and pure nitrogen (right column) interacting with (from top to bottom) c-SiO₂, a-SiO₂, h-SiO₂ and o-SiO₂.

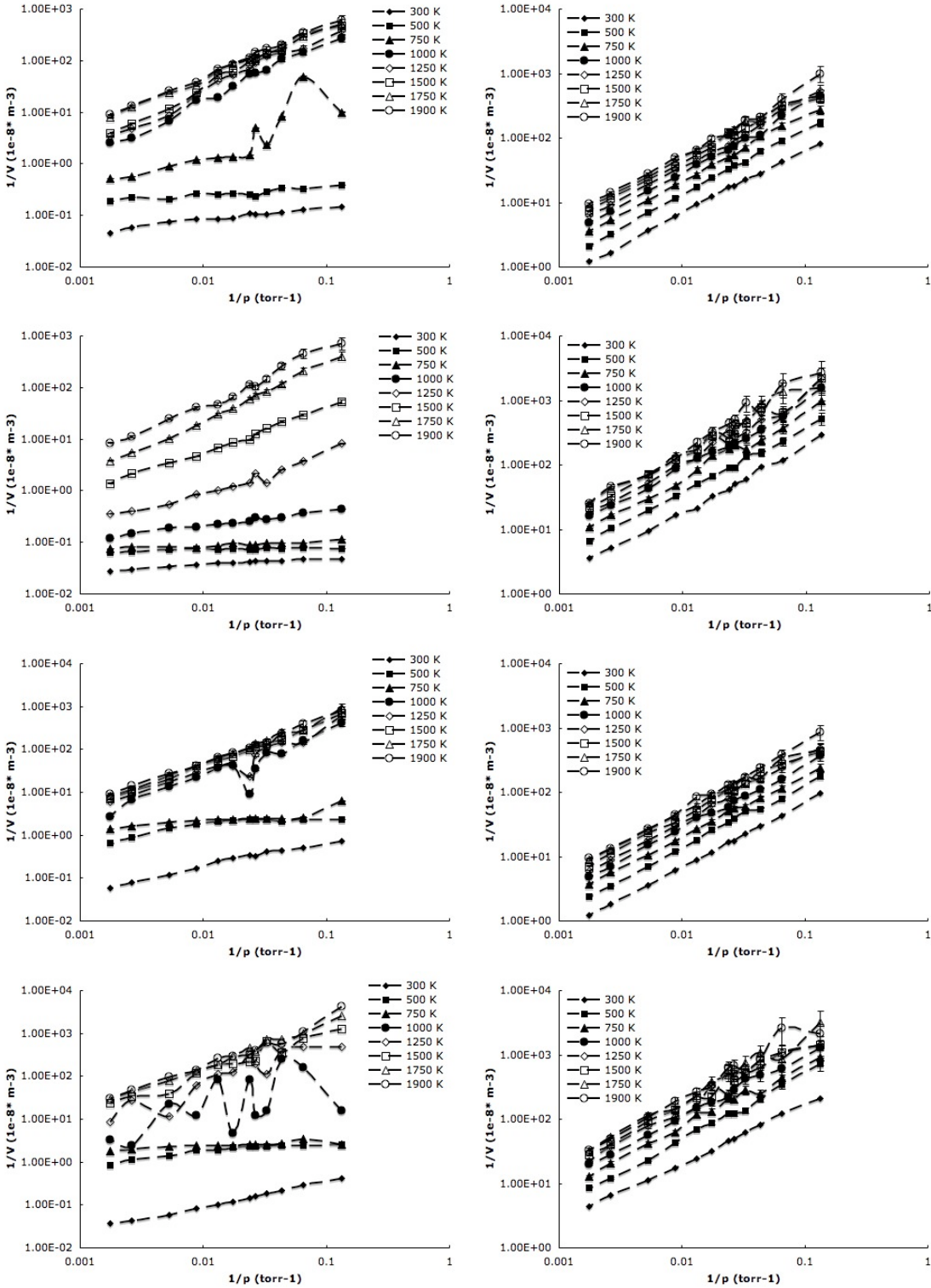


Figure 8. Log-Log plots of $(1/V, 1/p)$ for oxygen (left column) and nitrogen (right column) in an equal proportion mix interacting (from top to bottom) with c-SiO₂, a-SiO₂, h-SiO₂ and o-SiO₂.

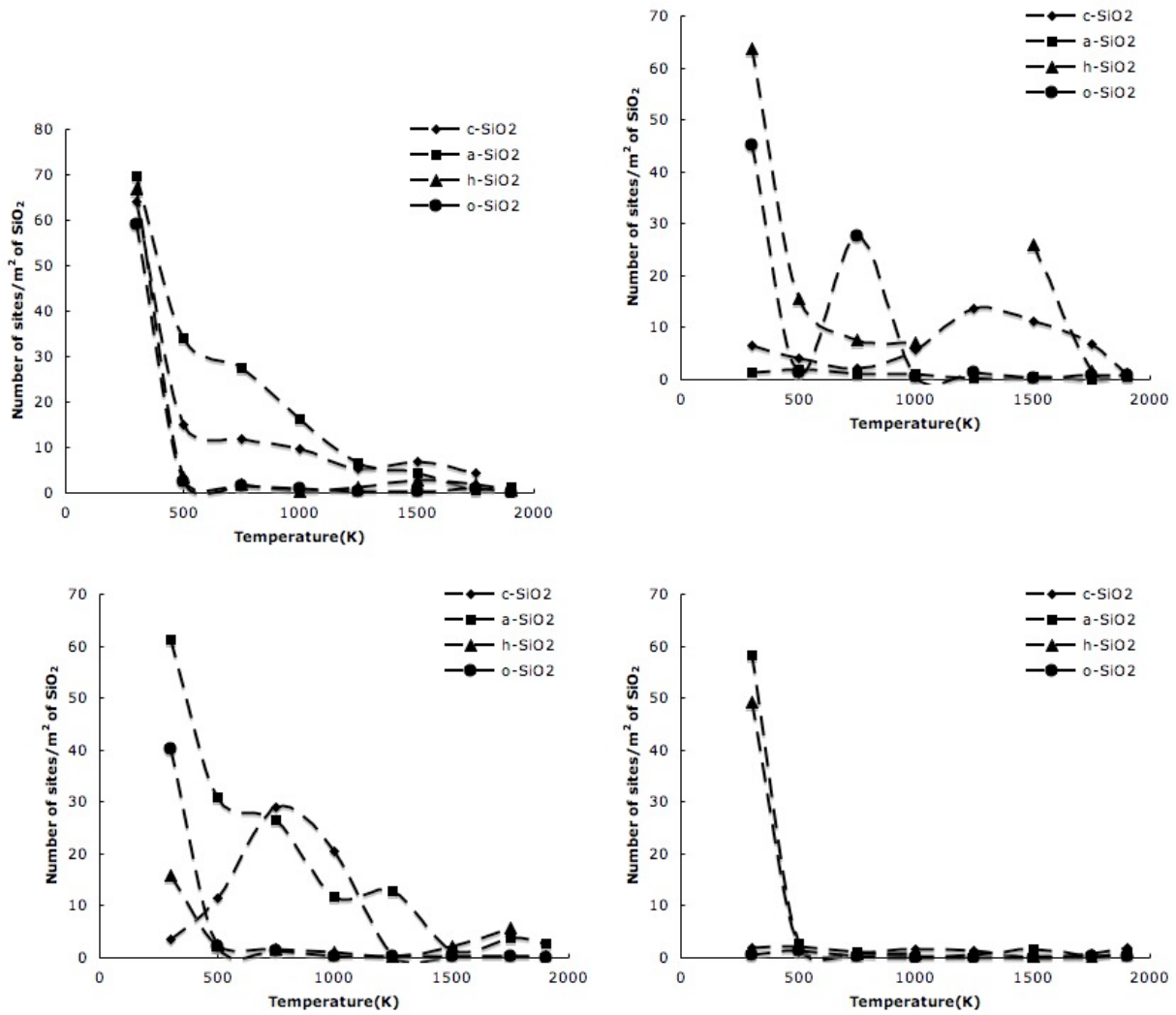


Figure 9. Temperature dependence of the number of adsorption sites per square meter of SiO₂ surface interacting with pure oxygen gas (top left), pure nitrogen gas (top right), oxygen in an ON gas mix (bottom left), and nitrogen in an ON gas mix (bottom right), as calculated from Grand Canonical Monte Carlo simulations. In all cases, adsorption of oxygen and nitrogen on various SiO₂ surfaces is significantly different at 300K compared to higher temperatures. The a-SiO₂ surface in general also adsorbs more oxygen and nitrogen compared to the c-SiO₂, while the h-SiO₂ and o-SiO₂ tend to reduce adsorption of oxygen and nitrogen on the solid substrate. Overall oxygen interactions with the SiO₂ surface are favored over nitrogen.

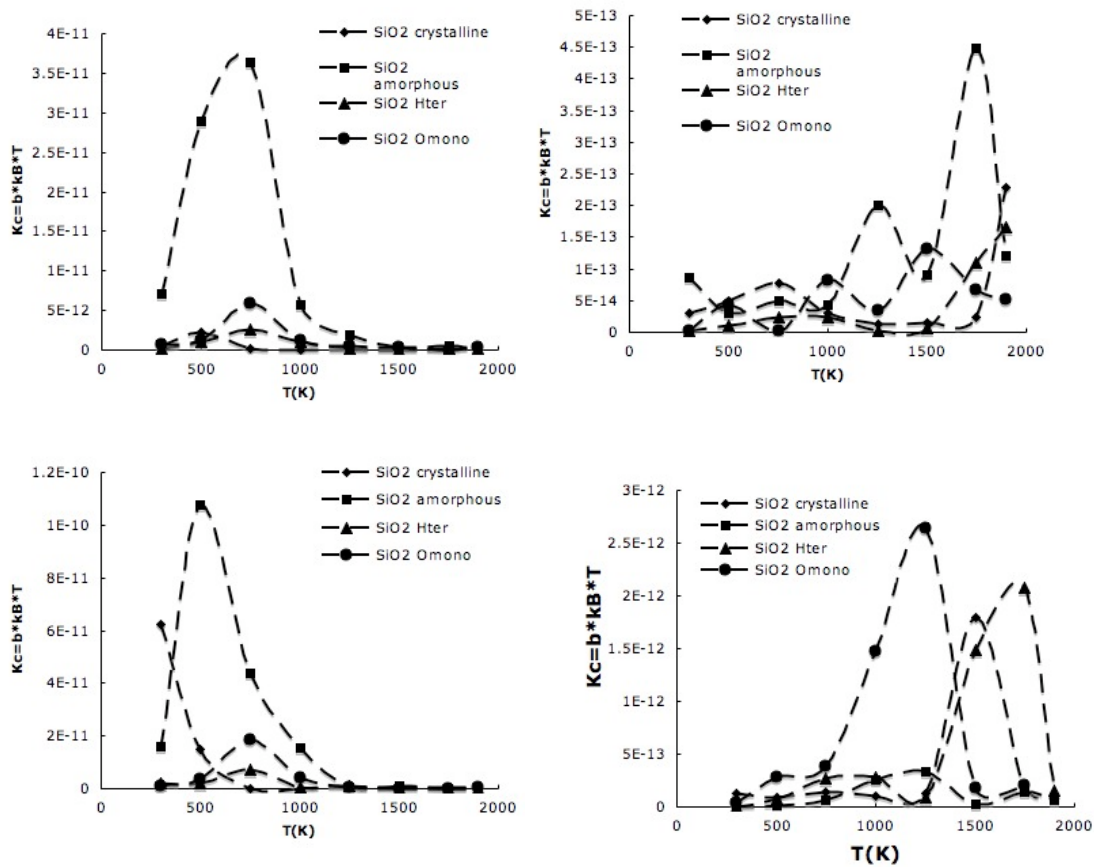
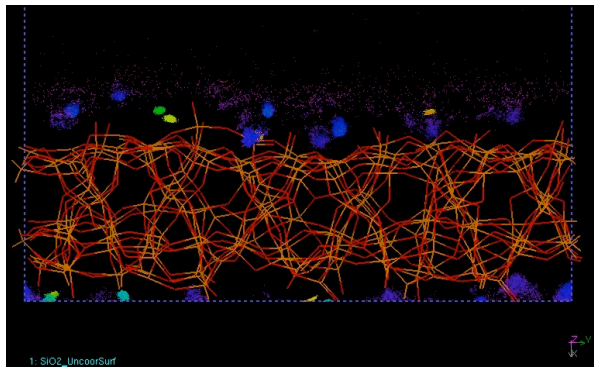
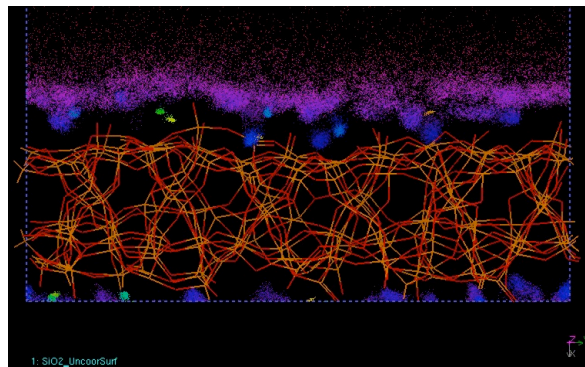


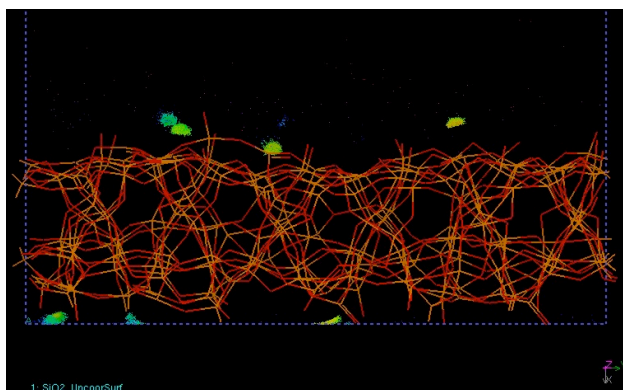
Figure 10. Equilibrium constants for pure oxygen (top-left), pure-nitrogen (top-right), oxygen in O/N mix (bottom left), and nitrogen in O/N mix (bottom right) adsorption on SiO₂.



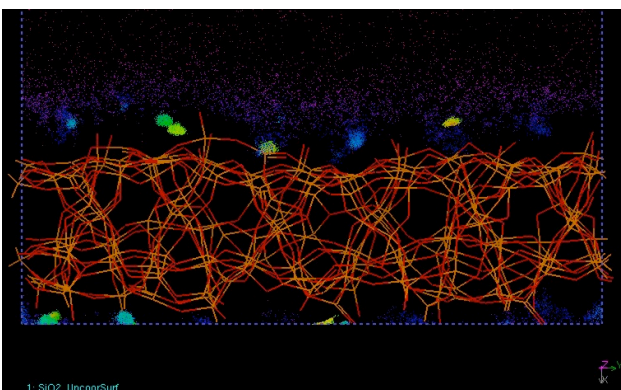
300K: 0.01 atm



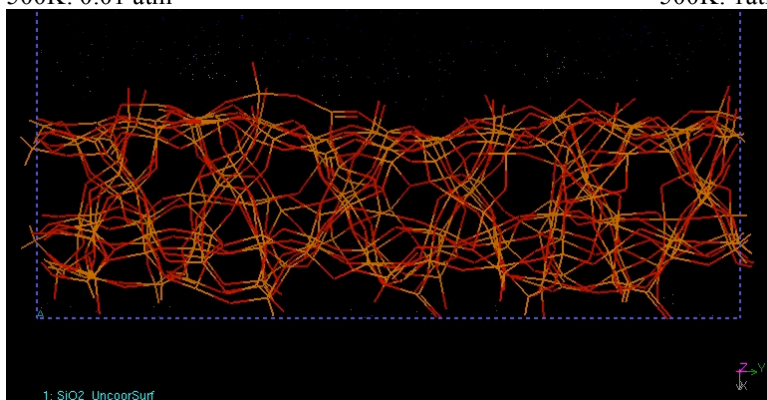
300K: 1 atm



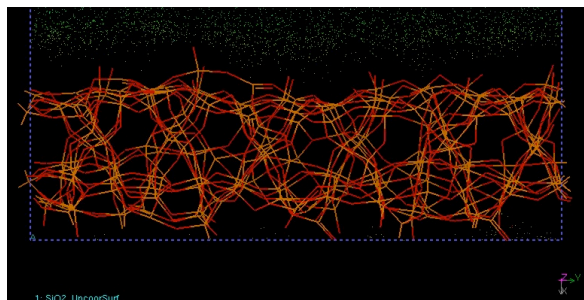
500K: 0.01 atm



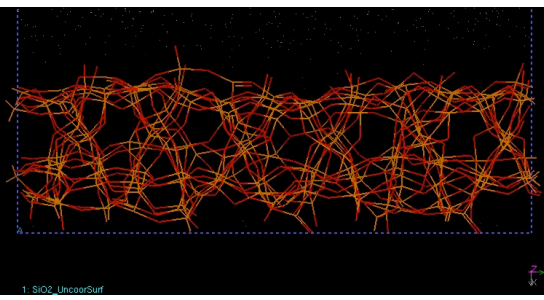
500K: 1 atm



1000K, 1 atm



300K: 1 atm



1000K: 1 atm

Figure 11. Distribution of adsorption sites for pure oxygen (top five images) and pure-nitrogen (bottom two images) on c-SiO₂.

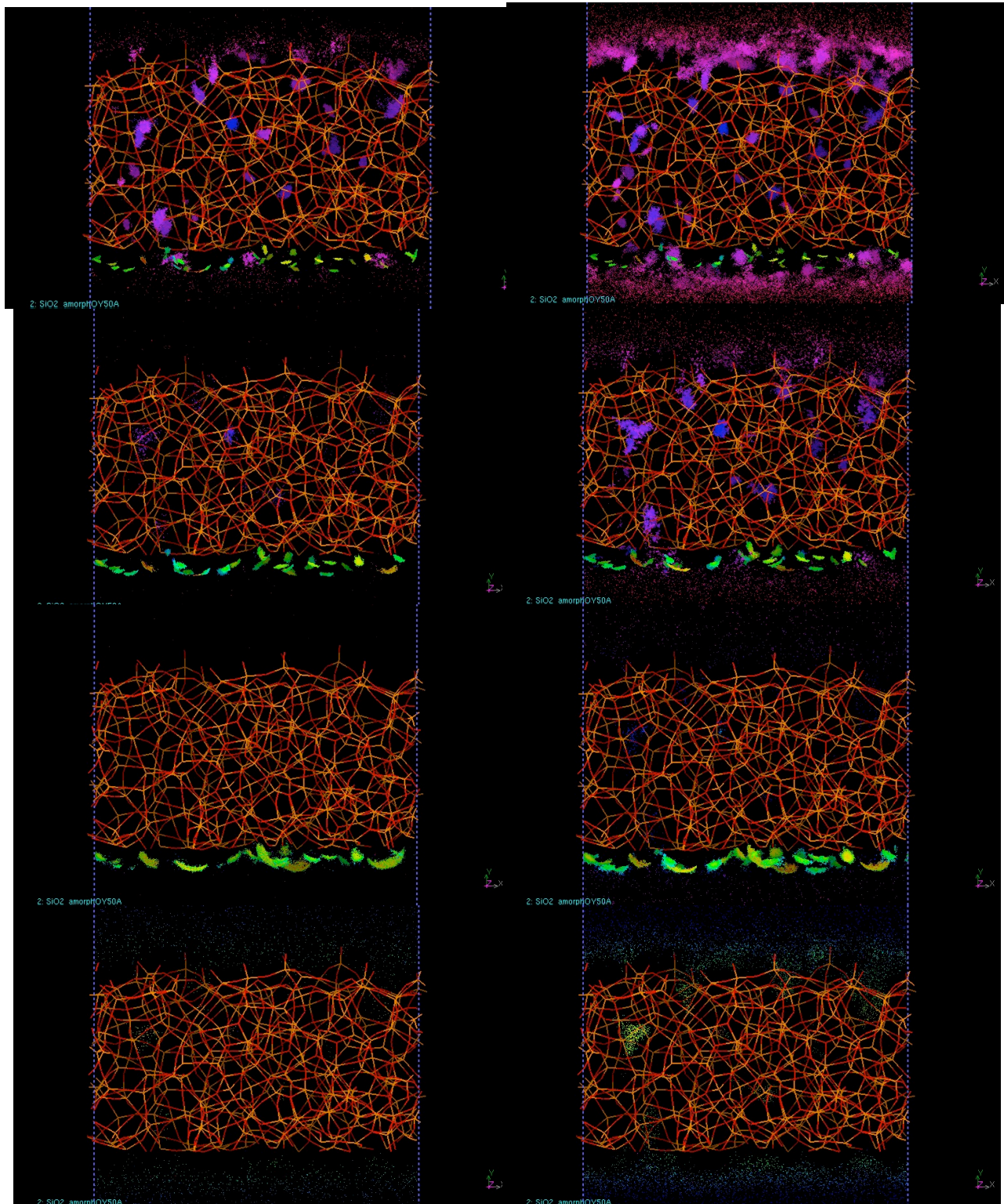


Figure 12. Distribution of adsorption sites on a-SiO₂. Pure oxygen (top six images: left column-0.01 atm, right column-1atm, first row-300K, second row-500K, third row-1000K) and pure-nitrogen (bottom two images: 300K and 0.01 atm-left, 1atm-right).

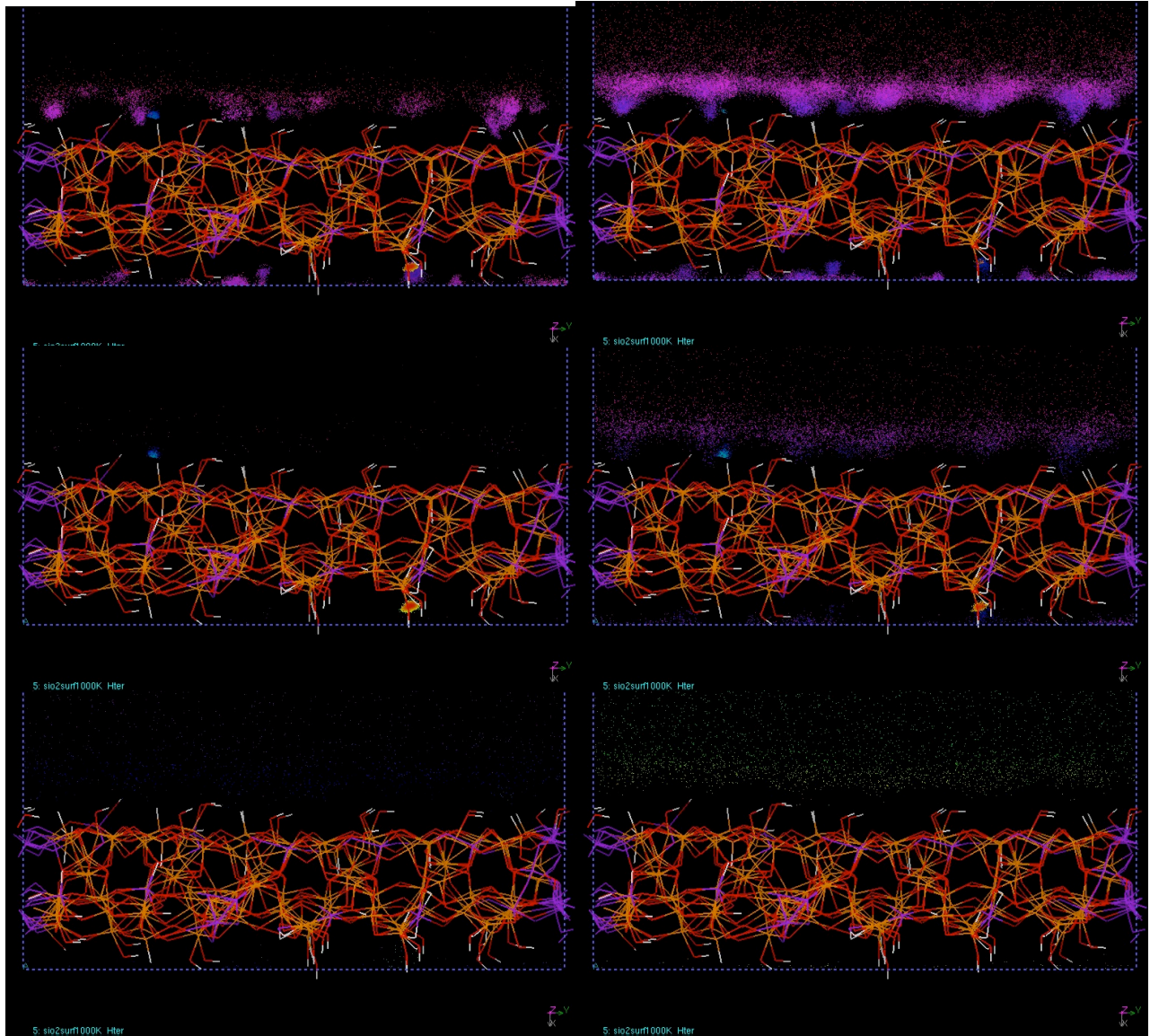


Figure 13. Distribution of adsorption sites on h-SiO₂. Pure oxygen (top four images: left column-0.01 atm, right column-1atm, first row-300K, second row-500K, bottom left: 1atm, 1000K) and pure-nitrogen (bottom right: 300K and 1atm).

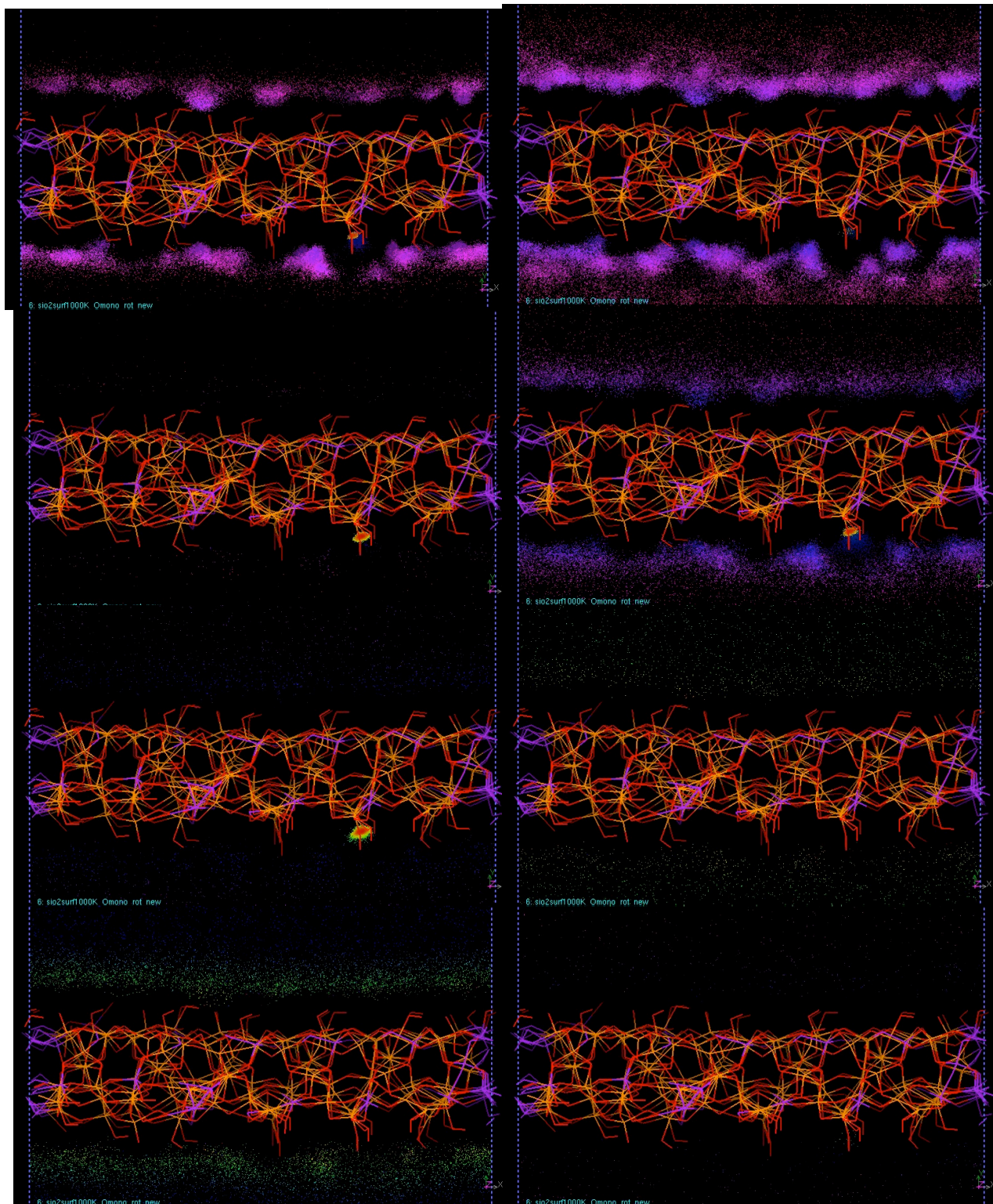


Figure 14. Distribution of adsorption sites on o-SiO₂. Pure oxygen (top four: left column-0.01 atm, right column-1atm, first row-300K, second row-500K, third row: 1atm, left: 1000K, right: 1900K) and pure nitrogen (bottom: 300K and 500K at 1atm).

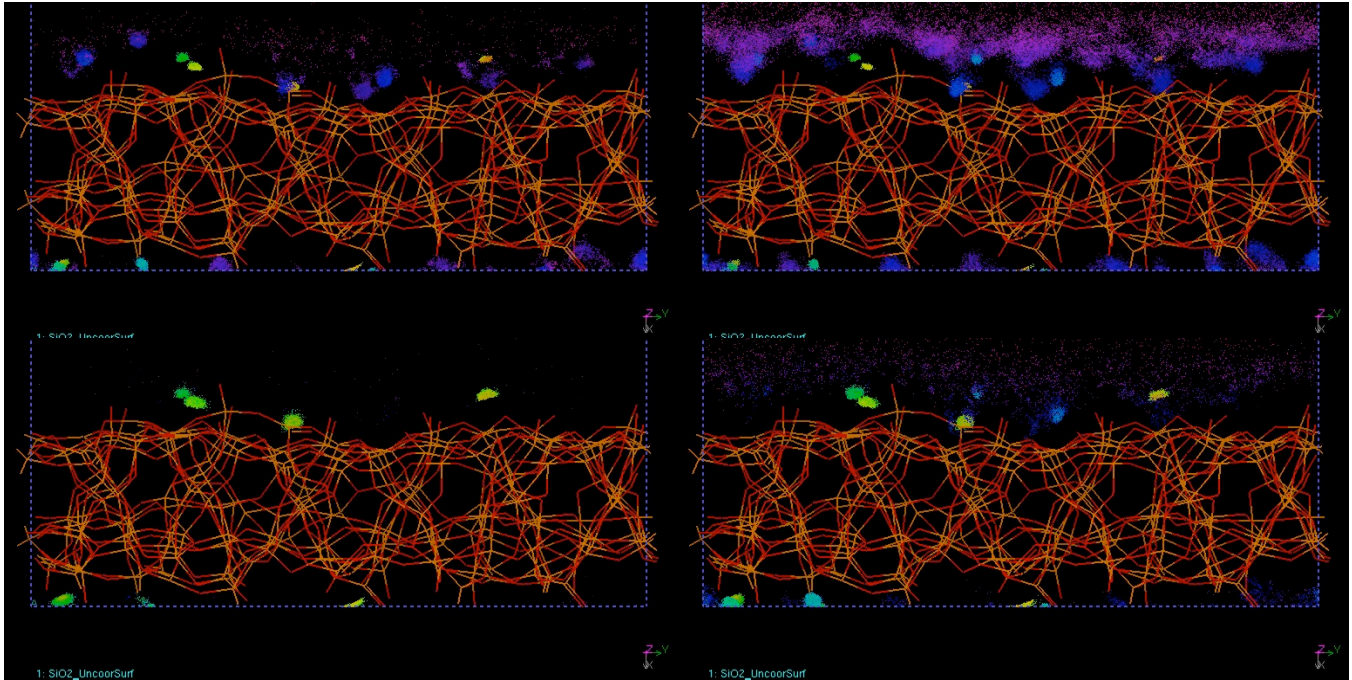


Figure 15. Distribution of adsorption sites on c-SiO₂ for O/N mix. Top row: 300K. Bottom row: 500K. Left column: 0.01 atm. Right column: 1 atm.

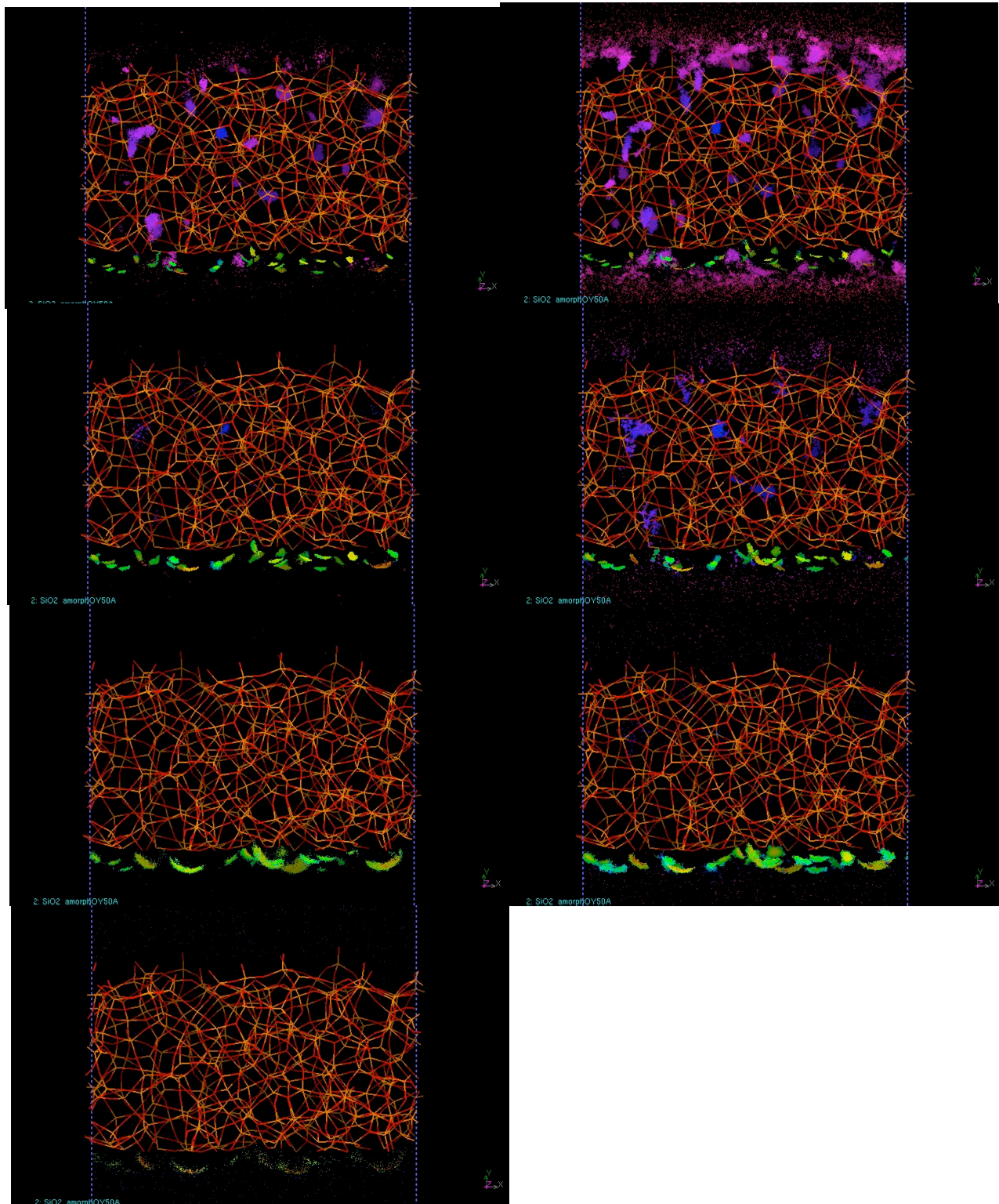


Figure 16. Distribution of adsorption sites on a-SiO₂ for O/N mix. First row: 300K. Second row: 500K. Third row: 1000K. Left column: 0.01 atm. Right column: 1 atm. Fourth row: 1900K and 1 atm.

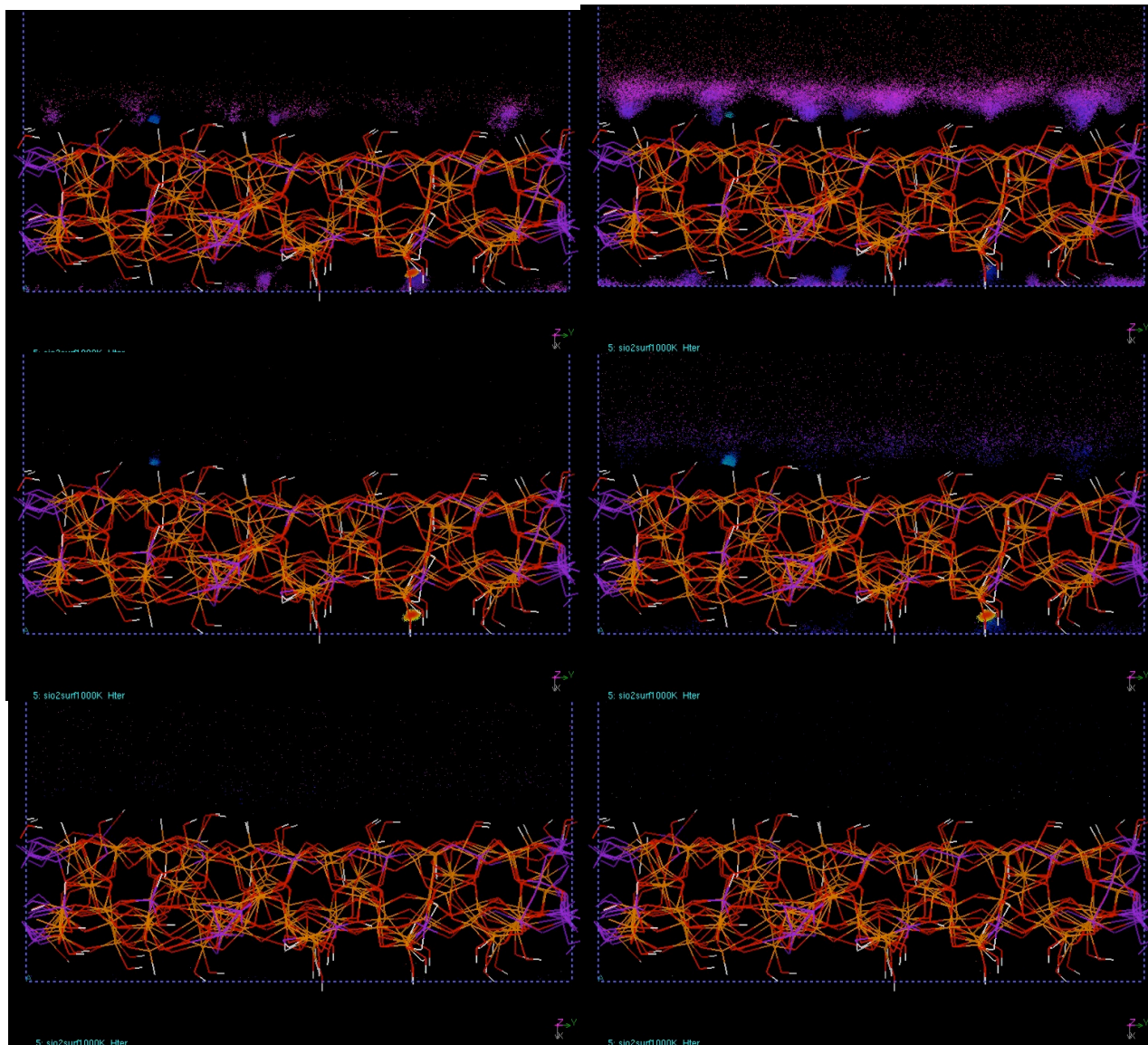


Figure 17. Distribution of adsorption sites on h-SiO₂ for O/N mix. First row: 300K. Second row: 500K. Left column: 0.01 atm. Right column: 1 atm. Third row: 1000K and 1atm. Fourth row: 1900K and 1 atm.

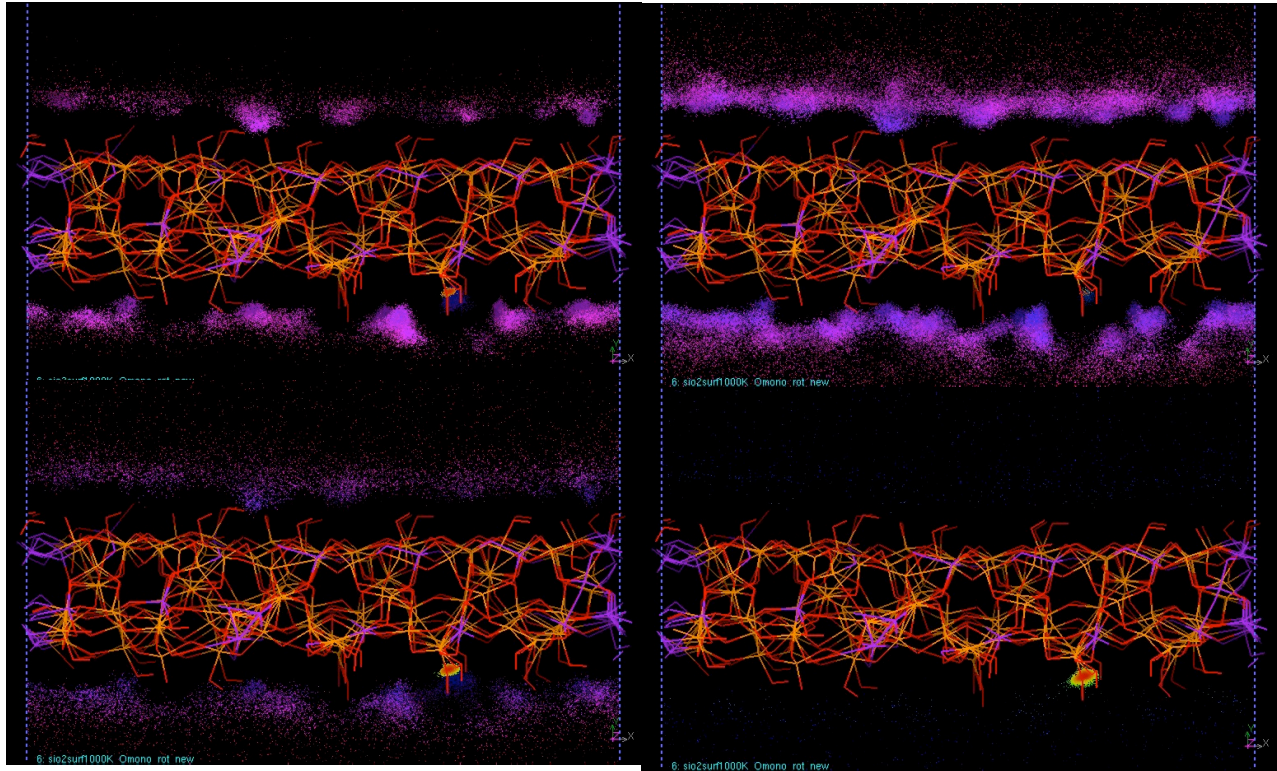


Figure 18. Distribution of adsorption sites on o-SiO₂ for O/N mix. Top row: 300K, 0.01 atm (left) and 1 atm (right). Bottom row: 1000K (left) and 1900K (right) at 1atm.

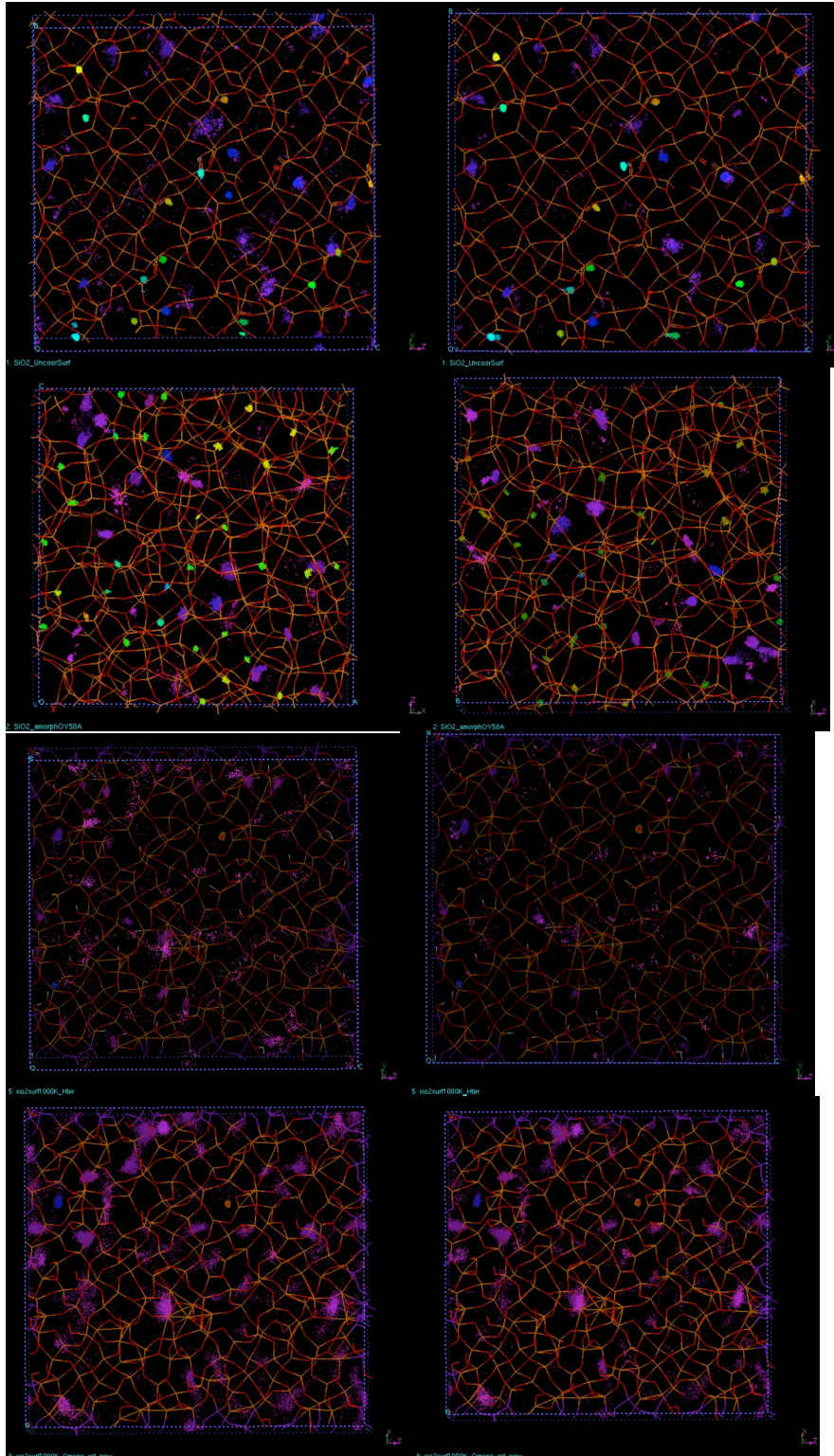


Figure 19. Top view of the distribution of adsorption sites for O/N mix at 300K and 0.01 atm (left column) and 1atm (right column) on c-SiO₂ (first row), a-SiO₂ (second row), h-SiO₂ (third row) and o-SiO₂ (fourth row).

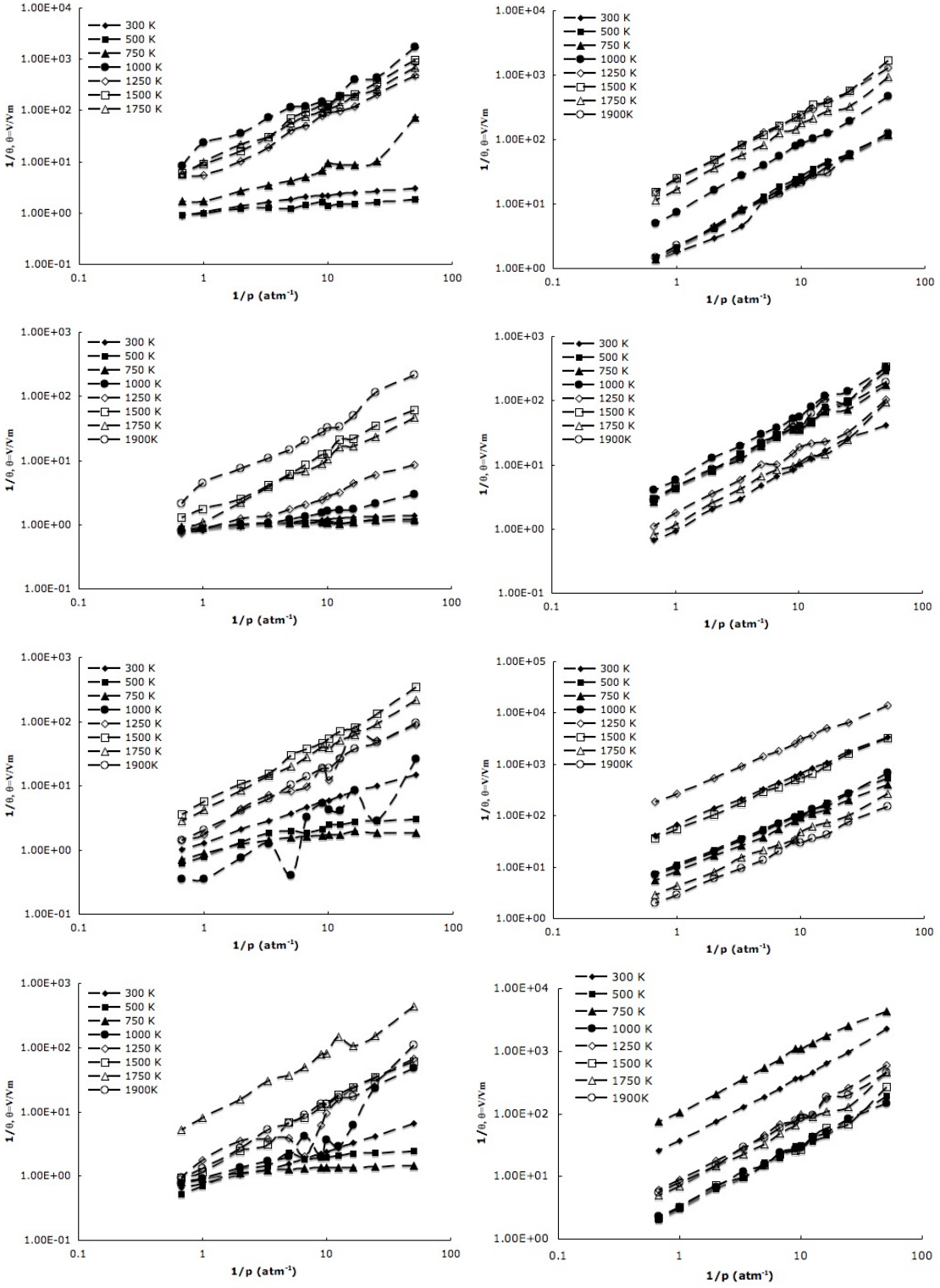


Figure 20. Adsorption isotherms (log-log plots) for pure oxygen (left column) and pure nitrogen (right column) on (from top to bottom) c-SiO₂, a-SiO₂, h-SiO₂, and o-SiO₂.

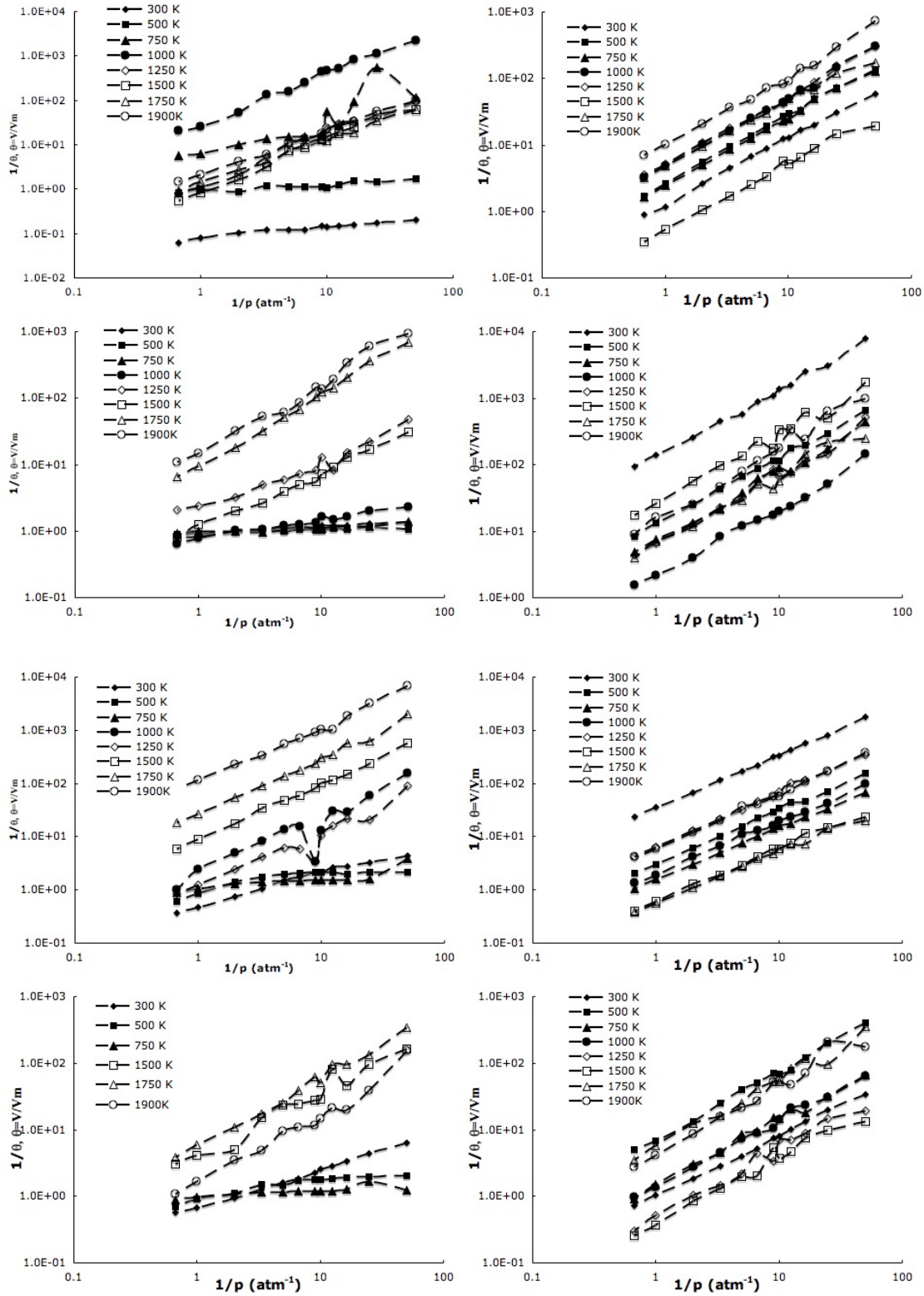


Figure 21. Adsorption isotherms (log-log plots) for oxygen in O/N mix (left column) and nitrogen in O/N mix (right column) on (from top to bottom) c-SiO₂, a-SiO₂, h-SiO₂, and o-SiO₂.

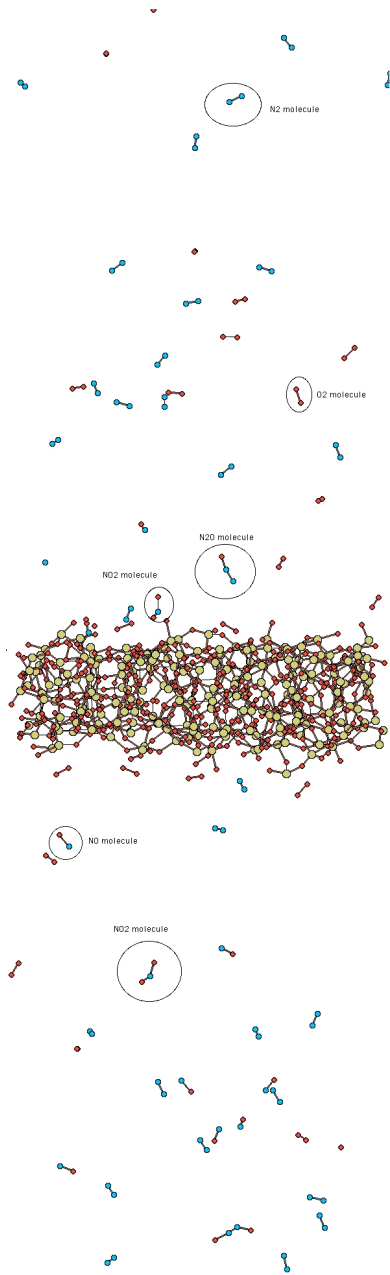


Figure 22. Snapshot from a Reactive Force Field Molecular Dynamics simulation at 1900K of SiO_2 (Si atoms are represented as yellow colored spheres) interacting with a mix of atomic nitrogen (blue spheres) and oxygen (red spheres) at 100atm. N_2 and O_2 molecules (characteristic for the gas phase chemistry) as well as NO , NO_2 , and N_2O , mostly surface mediated, can be observed (circled).

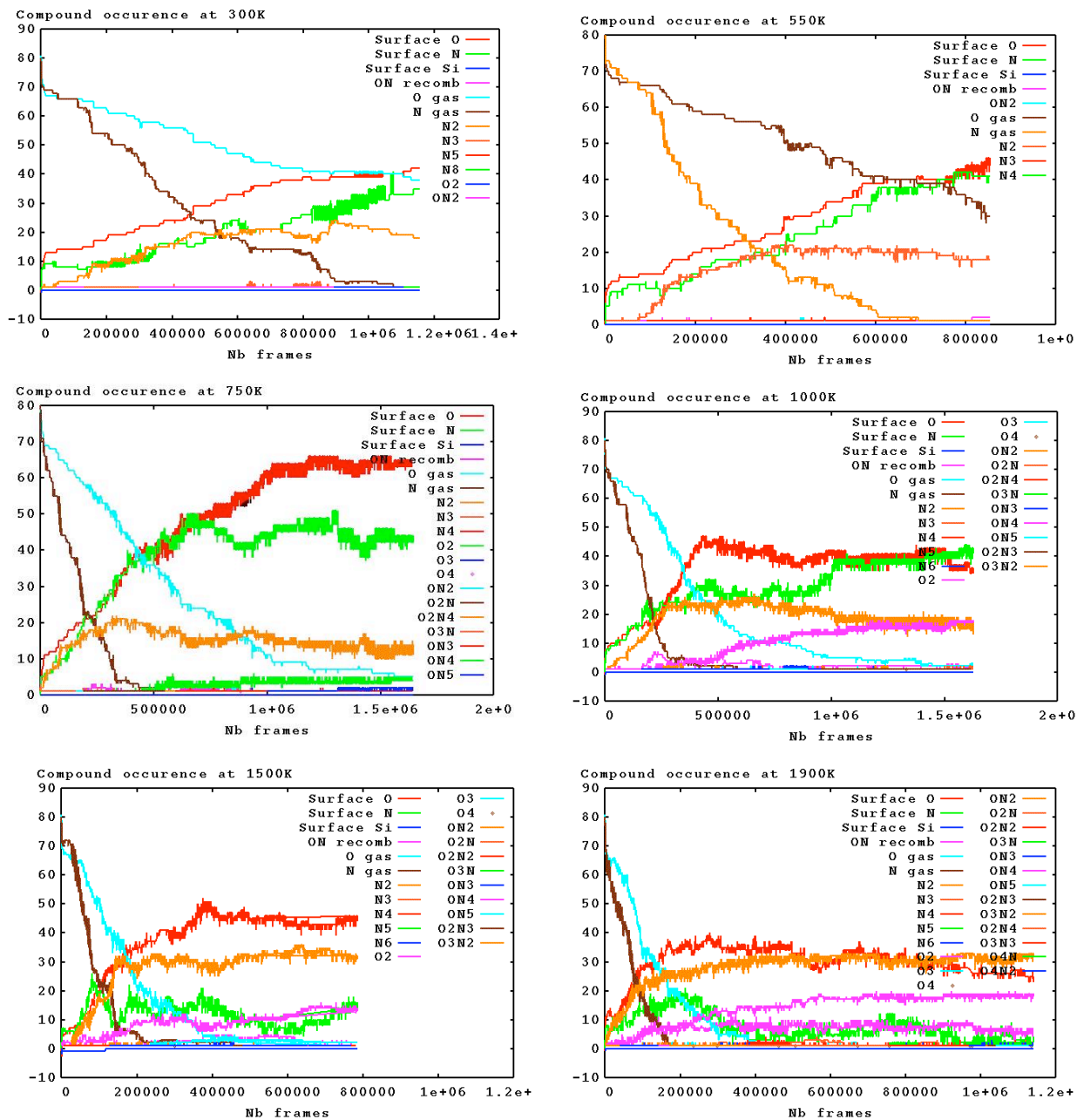


Figure 23. Compound occurrence from ReaxFF molecular dynamics simulations for crystalline SiO₂ surface at 100atm and temperatures of 300K, 550K, 750K, 1000K, 1500K and 1900K.

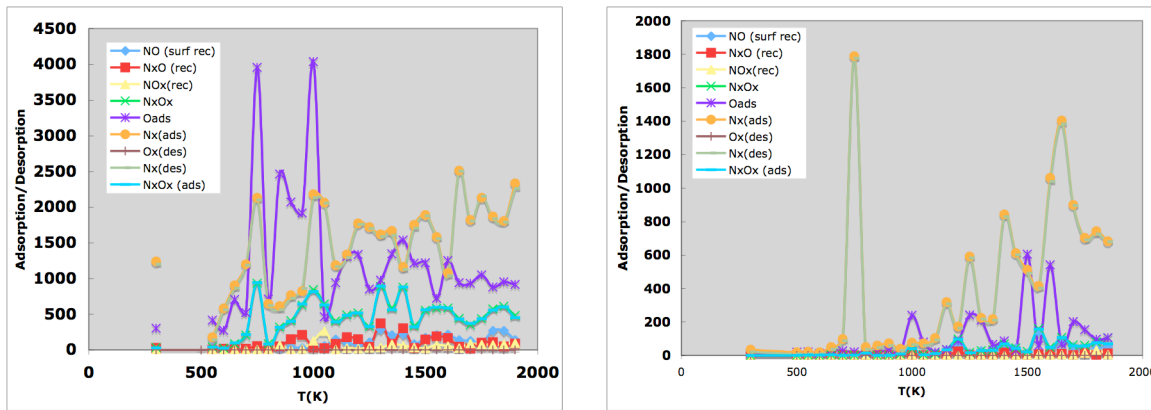


Figure 24. Surface mediated reactions as functions of temperature from ReaxFF molecular dynamics simulations for crystalline SiO₂ surface at 100atm (left) and 10atm (right).

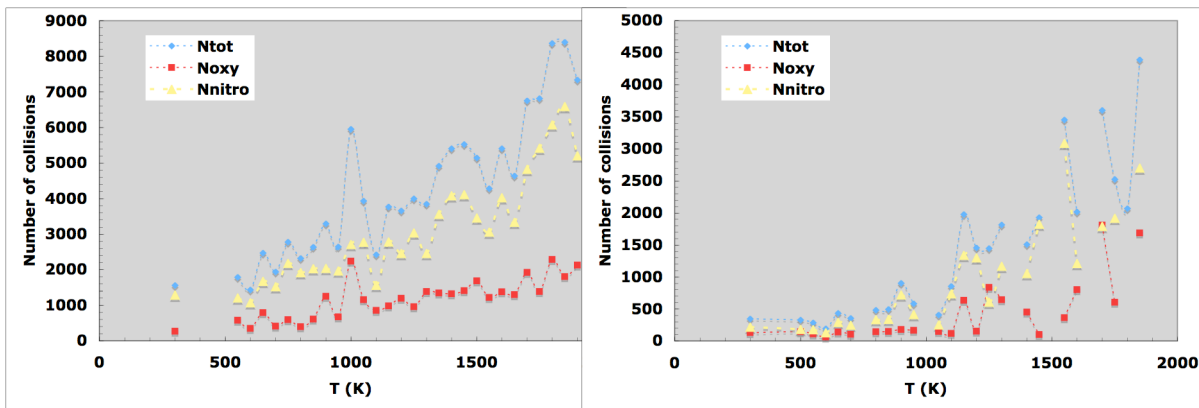


Figure 25. Number of collisions with crystalline SiO₂ surface as functions of temperature from ReaxFF molecular dynamics simulations at 100atm (left) and 10atm (right).

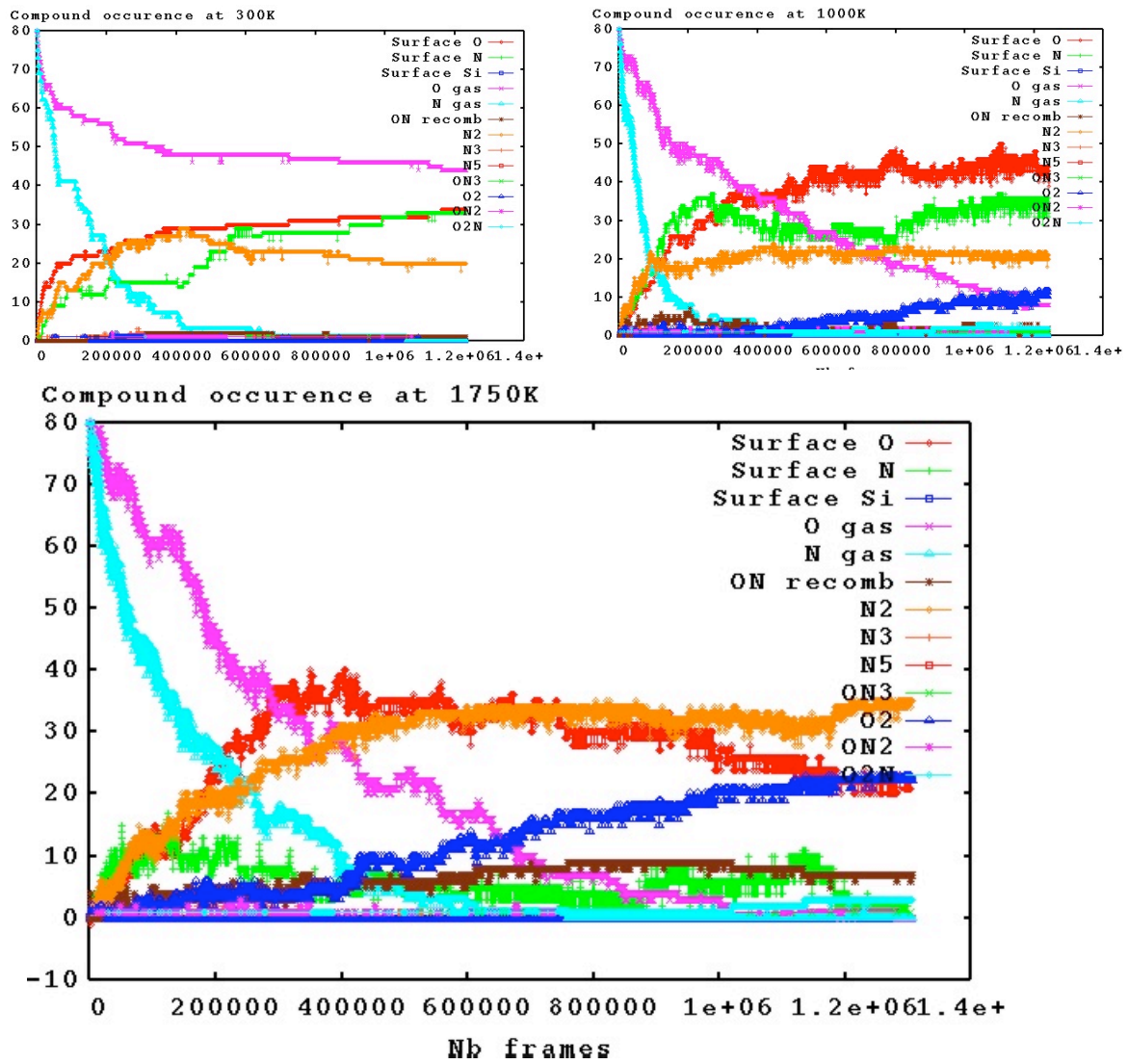


Figure 26. Compound occurrence from ReaxFF molecular dynamics simulations for amorphous SiO₂ surface at 100atm and temperatures of 300K, 550K, 750K, 1000K, 1500K, and 1900K.

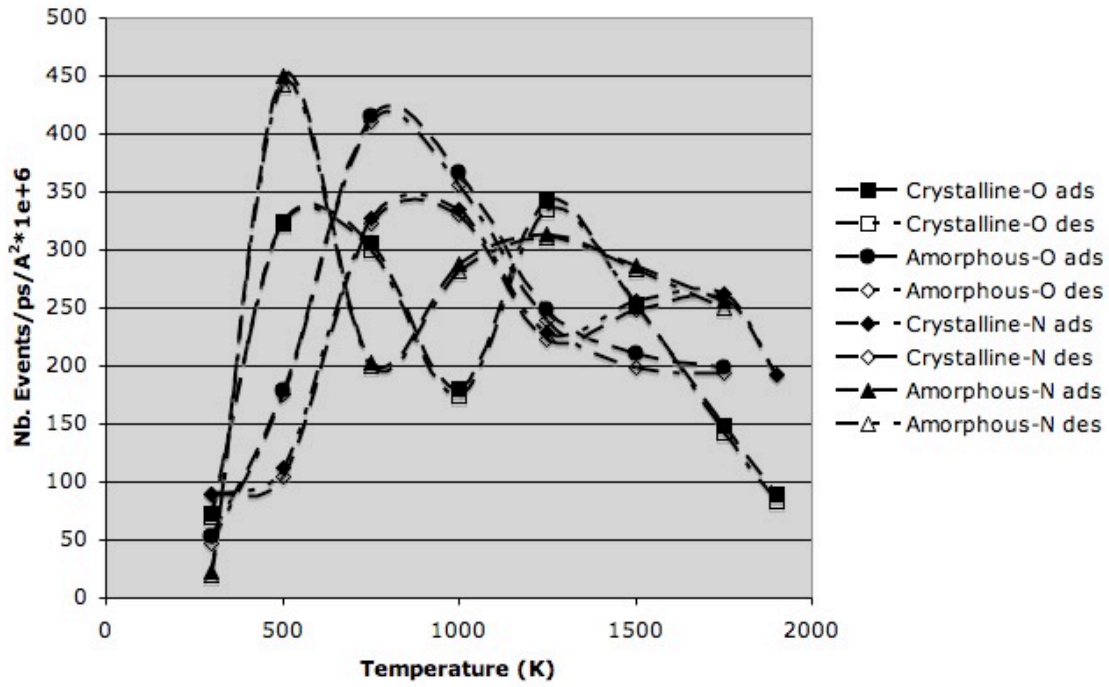


Figure 27. Temperature dependence of adsorption and desorption on crystalline and amorphous SiO₂ from ReaxFF MD simulations at 100atm.